ORIGINAL RESEARCH

# Combined Docetaxel/Pictilisib-Loaded mPEGylated Nanocarriers with Dual HER2 Targeting Antibodies for Synergistic Chemotherapy of Breast Cancer

Wei-Jie Cheng[1],*, Shyr-Yi Lin[2,3],*, Kuo-Hsiang Chuang[4,5],*, Michael Chen[4], Hsiu-O Ho ![ORCID][1], Ling-Chun Chen[6], Chien-Ming Hsieh ![ORCID][1], Ming-Thau Sheu ![ORCID][1]

[1]School of Pharmacy, College of Pharmacy, Taipei Medical University, Taipei, Taiwan; [2]Division of Gastroenterology, Department of Internal Medicine, Wan Fang Hospital, Taipei Medical University, Taipei, Taiwan; [3]Department of General Medicine, School of Medicine, College of Medicine, Taipei Medical University, Taipei, Taiwan; [4]Graduate Institute of Pharmacognosy, Taipei Medical University, Taipei, Taiwan; [5]PhD Program in Clinical Drug Development of Chinese Herbal Medicine, Taipei Medical University, Taipei, Taiwan; [6]Department of Biotechnology and Pharmaceutical Technology, Yuanpei University of Medical Technology, Hsinchu, Taiwan

*These authors contributed equally to this work

Correspondence: Chien-Ming Hsieh; Ming-Thau Sheu, Email cmhsieh@tmu.edu.tw; mingsheu@tmu.edu.tw

**Introduction:** Approximately 15%~30% of breast cancers have gene amplification or overexpression of the human epidermal growth factor receptor 2 (HER2), resulting in the chemotherapy resistance, a more-aggressive phenotype and poor prognosis.

**Methods:** We propose a strategy of nanocarriers co-loaded with docetaxel (DTX) and pictilisib (PIC) at a synergistic ratio and non-covalently bound with dual anti-HER2 epitopes bispecific antibodies (BsAbs: anti-HER2-IV/methoxy-polyethylene glycol (mPEG) and anti-HER2-II/methoxy-PEG) for synergistic targeting to overcome the therapeutic dilemmas of the resistance for HER2-targetable chemodrugs. DTX/PIC-loaded nanocarriers (D/P_NCs) were prepared with single emulsion methods and characterized using dynamic light scattering analysis, and the drug content was assayed by high-performance liquid chromatographic method. The integrity and function of BsABs were evaluated using sodium dodecylsulfate polyacrylamide gel electrophoresis (SDS-PAGE) and enzyme-linked immunosorbent assay (ELISA). The in vitro cell studies and in vivo breast tumor-bearing mice model were used to evaluate the anti-cancer effect and biosafety of formulations.

**Results:** D/P_NCs optimally prepared exhibited a spherical morphology with small particle sizes (~140 nm), high drug loading (~5.5%), and good colloidal stability. The synergistic tumor cytotoxicity of loading DTX and PIC at 2:1 ratio in D/P_NCs was discovered. The BsAbs are successfully decorated on mPEGylated DTX/PIC-loaded nanocarriers via anti-mPEG moiety. In vitro studies revealed that non-covalent decoration with dual BsAbs on D_P-NCs significantly and synergistically increased cellular uptake, while with loading DTX and PIC at a synergistic ratio of 2:1 in D/P_NCs further resulted in synergistic cytotoxicity. In vivo tumor inhibition studies showed the comparable results for synergistic antitumor efficacy while minimizing systemic toxicity of chemodrugs.

**Conclusion:** Non-covalent modification with dual distinct epitopes BsAbs on the nanocarriers loaded with dual chemodrugs at a synergistic ratio was expected to be a promising therapeutic platform to overcome the chemoresistance of various cancers and warrants further development for future therapy in the clinical.

**Keywords:** docetaxel, pictilisib, nanocarriers, bispecific antibodies, dual epitopes, HER2-positive breast cancer

## Introduction

Breast cancer is the predominantly diagnosed cancer in women and also the leading cause of female cancer deaths.[1,2] Approximately 15%~30% of breast cancers have gene amplification or overexpression of the human epidermal growth factor receptor 2 (HER2), resulting in a more-aggressive phenotype and poor prognosis. HER2, also known as erbB2, belongs to a family of tyrosine kinases and regulates cell proliferation, survival, and metastasis of cancer cells.[3–5] Hence, several anti-HER2 agents were developed, including monoclonal antibodies, tyrosine kinase inhibitors, and antibody-drug

**Graphical Abstract**
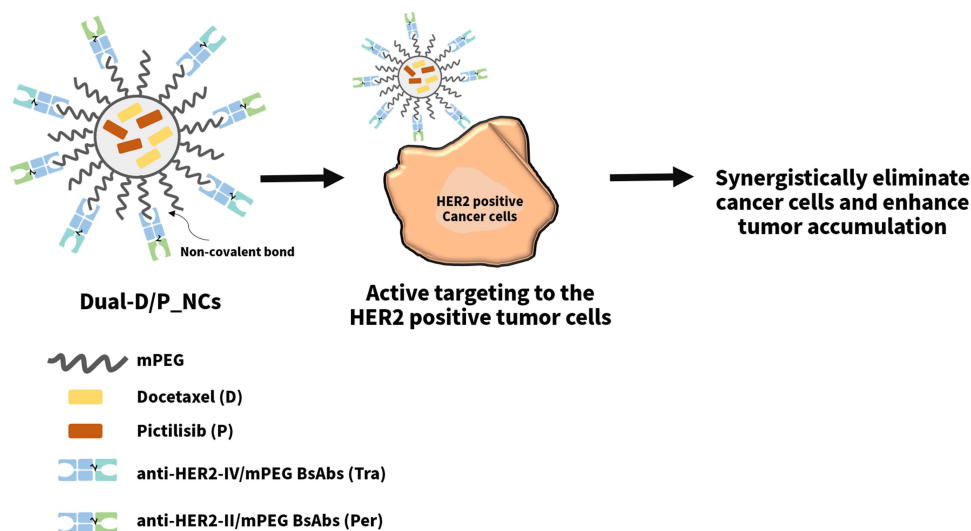


conjugates (ADCs).[6,7] Trastuzumab, the first anti-HER2 humanized monoclonal antibody, binds subdomain IV of the HER2 extracellular domain, which blocks dimerization of the ligand-independent HER2 receptor and inhibits downstream signal transduction pathways and induction of apoptosis.[8] Several clinical trials reported that adding trastuzumab to chemotherapy substantially improved overall survival and was particularly more effective with taxane.[9,10] Therefore, adjuvant chemotherapy with taxane and trastuzumab became first-line treatment for HER2-positive breast cancer.[11] Additionally, pertuzumab binds subdomain II of the HER2 extracellular domain, which blocks ligand-dependent HER2 heterodimerization and thus inhibits tumor proliferation.[12] Due to the different binding epitopes of HER2, the mechanisms of action of trastuzumab and pertuzumab are complementary. Combining the two antibodies resulted in comprehensive blockade of HER2 signaling, which synergistically enhanced the antitumor efficacy in HER2-positive breast cancer.[13–15] Furthermore, the combination of pertuzumab, trastuzumab, and docetaxel (DTX) significantly prolonged progression-free survival and overall survival of patients with HER2-positive metastatic breast cancer.[16]

The phosphatidylinositol 3-kinase (PI3K) pathway is the major downstream signaling pathway of several growth factor receptors, such as HER2, epidermal growth factor receptor (EGFR), and other receptor tyrosine kinases.[17] The PI3K pathway plays a key role in regulating cell proliferation, apoptosis, and metabolism.[18,19] Mutation or amplification of the phosphatidylinositol-4,5-bisphosphate 3-kinase, catalytic subunit alpha (*PIK3CA*) gene, a subunit of PI3K, occurs in nearly 25% of HER2-positive breast cancers, and is associated with resistance to endocrine therapy and anti-HER2-targeted agents, resulting in a poor prognosis.[20–22] It was demonstrated that a combination of anti-HER2-targeted therapy and PI3K inhibitors overcame resistance and enhanced the antitumor therapeutic activity in HER2-positive breast cancer.[23–25] Pictilisib (PIC) is a potent selective pan-inhibitor of class 1 PI3K, and it exhibited good antitumor efficacy, safety, and tolerance in clinical trials.[26–28] It was also demonstrated that the addition of PIC to DTX or trastuzumab, and pertuzumab could augment the antitumor effect in breast cancer cells.[29,30] Furthermore, recent findings revealed that PIC significantly increased cluster of differentiation 8-positive (CD8$^+$) T-cell infiltration, which may potentiate immune surveillance of breast cancer.[31]

With the rapid development of nanotechnology, the nanocarriers have been widely used as promising controlled drug delivery systems (DDS) to increase the efficacy and treat variety of cancer and other diseases.[32–35] Compared with the free drugs, the nanoparticles-based DDS offers several advantages, such as increase of site-specific accumulation and drug half-life, decrease of toxicity, improvement of stability and solubility of hydrophobic drugs and protection of sensitive cargos (eg, mRNA).[36,37] Although most of these materials for nanocarriers are

biocompatible and biodegradable, these nanocarriers are still easily opsonized and recognized by the immune system, leading to the rapid clearance from the bloodstream.[38] To conquer obstacles, PEGylation, the covalent attachment of polyethylene glycol (PEG) chains, has been reported and widely used to hinder the nanoparticles to reduce the protein absorption and increase the stability, resulting in prolonging the in vivo circulation time.[39–41] Particularly, the PEGylated lipids, such as 1,2-Distearoyl-sn-glycero-3-phosphoethanolamine-N-[methoxy(polyethylene glycol)-2000] (DSPE-mPEG2k), are considered as biocompatible materials and also widely utilized in the preparation of several Food and Drug Administration (FDA) approved nanomedicines, such as Doxil® and Comirnaty®.[42,43]

Hence, to conquer these clinical dilemmas of breast carcinoma treatment, including the resistance of anti-HER2-targeted agents and chemotherapy, we aimed to develop a nanoplatform, which combined the taxane and PI3K inhibitor with the HER2-directed therapies. Herein, we developed dual bispecific antibodies (BsAbs, anti-HER2-IV/methoxy(polyethylene glycol (mPEG)) and anti-HER2-II/mPEG)-decorated DTX (D)/PIC (P)-loaded nanocarriers (Dual-D/P-NCs) to achieve a synergistic antitumor effect. We prepared DTX/PIC-loaded nanocarriers (D/P_NCs) using a single emulsion method and assessed the physical characterization and stability of D/P_NCs. The BsAbs were designed and prepared. In addition, the functionality and integrity of both BsAbs were verified by flow cytometry and sodium dodecylsulfate polyacrylamide gel electrophoresis (SDS-PAGE). Then, we evaluated the cellular uptake and cytotoxicity of the Dual-D/P_NCs. At last, in vivo studies were conducted to evaluate the biodistribution, antitumor efficacy, and biosafety of the Dual-D/P_NCs.

## Materials and Methods
### Cell Culture
The MCF-7/HER2 cell line was kindly provided by Dr Mien-Chie Hung (Houston, TX, USA). The MCF-7 and NIT/3T3 cell lines were obtained from American Type Culture Collection (Manassas, VA, USA). The use of the cell line and cell experiments was reviewed and approved by the Institutional Animal Care and Use Committee of Taipei Medical University (LAC-2021-0231). The MCF-7 and NIT/3T3 cell lines were cultured in DMEM supplemented with 10% FBS and 1% penicillin/streptomycin/amphotericin B. MCF-7/HER2 cells were cultured in DMEM/F12 medium supplemented with 10% FBS and 1% penicillin/streptomycin/amphotericin B. These cells were incubated at 37 °C in a humidified 5% $CO_2$ air.

### Preparation of DTX/PIC-Loaded Nanocarriers, DIO-Loaded Nanocarriers and Dual BsAb-Decorated DTX/PIC-Loaded Nanocarriers
The emulsion technique was the common method of preparation of nanocarriers, which can be divided into single or double emulsion methods.[44,45] To encapsulate the docetaxel and pictilisib simultaneously, D/P_NCs were prepared using an oil-in-water single emulsion. Initially, 1.5 mg of chemodrugs and 15 mg of DSPE-mPEG2k were dissolved in 1 mL of chloroform. Soybean lecithin (S100) was suspended in 10 mL of deionized water and then subjected to ultrasonication (VCX 750; Sonics & Materials, Newtown, CT, USA) to form a nanosuspension. The chloroform solution was added to the nanosuspension, and the probe sonicator was set to a level at 150 W and six pulses of 10s to form the emulsion. The emulsion was subsequently stirred at 500 rpm for 3 h to completely remove the organic solvents. An appropriate amount of trehalose as the cryoprotectant was added to the solution, and unencapsulated drugs were discarded by filtering the solution through a 0.45-μm membrane filter (Millipore, Billerica, MA, USA). After lyophilization, the lyophilized product was stored at 4 °C until use. For in vitro cellular uptake studies, DIO-loaded nanocarriers (DIO_NCs) were prepared following the same protocol instead of encapsulating DTX or PIC. Instead, the 1.5 mg of DIO and 15 mg of DSPE-mPEG2k were dissolved in 1 mL of chloroform. To produce the BsAb-decorated D/P_NCs, the D/P_NCs were incubated with anti-HER2-IV/mPEG (Tra) and/or anti-HER2-II/mPEG (Per) in a 0.05% (w/w) BSA/phosphate-buffered saline (PBS) buffer solution for 30 min at room temperature to enable the BsAbs to non-covalently decorate the D/P_NCs via the anti-mPEG fragments of the BsAbs.

# Physical Characterization of DTX/PIC-Loaded Nanocarriers and Dual BsAb-Decorated DTX/PIC-Loaded Nanocarriers

The particle size and zeta potential (ZP) were measured with a Zetasizer ZSP (Malvern Instruments, Malvern, UK) at 25 °C. Images of the morphology of the D/P_NCs were produced by transmission electron microscopy (TEM) (HT7700, Hitachi, Tokyo, Japan). In brief, D/P_NCs solution was dropped onto a formvar/carbon-coated copper grid and allowed to stand for 2 min. Then, 2% uranyl acetate was dropped onto the grid and allowed to stand for 5 min. The grid was dried in advance of the TEM analysis. The encapsulation efficiency (EE) and drug loading (DL) of DTX and PIC were analyzed using the high-performance liquid chromatography (HPLC, Jasco, Tokyo, Japan), which was equipped with an Inertsil® ODS-3 column (4.6 mm × 15 cm; 5 μm). The detection wavelength was 227 nm, the flow rate was 1 mL/min, and the mobile phase was composed of 45% acetonitrile (ACN) and 55% deionized water. The EE (%) and DL (%) were respectively calculated using the following formula:

EE = (amount of measured drugs/amount of drugs added) × 100% and

DL = (amount of measured drugs/weight of NCs) × 100%.

# Preparation and Functionality Study of Anti-HER2-IV/mPEG and Anti-HER2-II/mPEG BsAbs

The anti-HER2-IV/mPEG (Tra) and anti-HER2-II/mPEG (Per) BsAbs were constructed from the same fragment antigen-binding (Fab) fragment of the humanized anti-mPEG and the single-chain variable fragment (scFv) of trastuzumab (anti-HER2-IV) and pertuzumab (anti-HER2-II), respectively. The anti-HER2-IV/mPEG BsAbs (Tra) were developed in a previous study,[46] and the anti-HER2-II/mPEG BsAbs (Per) were prepared by a similar process with the minor difference of the scFv.[47] Briefly, the BsAb gene construct was inserted into the pLNCX vector. Then, the plasmids were transfected into Expi293 cells using an Expi293™ Expression System Kit for large-scale production. After around 6 days, the BsAbs in the supernatant of the medium were collected and purified with a HisTrap HP column (GE Healthcare, Little Chalfont, UK). The integrity and purity of the BsAbs were assessed using non-reducing and reducing SDS-PAGE. The functionality of the anti-HER2 and anti-mPEG of the BsAbs was respectively assessed by flow cytometry and an enzyme-linked immunosorbent assay (ELISA). To determine the binding specificity of anti-HER2, MCF-7/HER2 cells were used, and NIH/3T3 cells, which are mouse embryonic fibroblasts, were used as the negative control. After being incubated with the cells, the BsAbs on the cells were labeled with goat anti-human IgG F(ab')2-FITC. The FITC fluorescence was analyzed by a Sony SA3800 Spectral flow cytometer (Sony, Tokyo, Japan). To confirm the binding specificity of anti-mPEG, Nunc-Immuno plates (ThermoFisher Scientific) were coated with 20 μg/mL of mPEG2k-NH2 or BSA at 37 °C for 2 h. After the ELISA plates were blocked with 5% skimmed milk and washed with PBS, graded concentrations of Tra or Per BsAbs were added to the wells and incubated for 1 h. After the plates were washed with PBS, goat anti-Human IgG Fab HRP was added to the wells, and 0.4 mg/mL of ABTS substrate solution was subsequently added to the wells. After incubation at 25 °C for 30 min, the absorbance was measured at 405 nm using ELISA reader (Cytation 3; BioTek Instruments, Winooski, VT, USA).

# Optimization of the Binding Molar Ratio of BsAbs to DTX/PIC-Loaded Nanocarriers

To evaluate the optimal-binding ratio of BsAbs to DSPE-mPEG2k of the D/P_NCs, D/P_NCs were incubated with Per BsAbs at different DSPE-mPEG2 to BsAbs molar ratios of 50:1, 100:1, 500:1, and 1000:1; the excess unbound BsAbs were detected by ELISA. Briefly, Nunc-Immuno plates (ThermoFisher Scientific, Waltham, MA, USA) were coated with 50 μL of 20 μg/mL of mPEG2k-NH2 at 37 °C for 2 h. Skimmed milk (5%; 200 μL) in PBS as a blocking buffer was added to each well at 4 °C overnight. Further, each well was washed thrice with PBS. Different molar ratios of Per-D/P_NCs were diluted with 2% skimmed milk in PBS to 0.0032~2 μg/mL of BsAbs. About 50 μL each of diluted BsAbs-D/P_NCs, D/P_NCs, and Per BsAbs was added to a 96-well plate and incubated for 1 h. Then, the wells were washed with PBS to remove any excess BsAbs. About 50 μL of goat anti-human IgG F(ab')2-HRP in 2% (w/v) skimmed milk/PBS was added to the wells for 1 h at room temperature. After the wells were washed with PBS five times, 150 μL of

a 0.4 mg/mL ABTS solution in 0.01% $H_2O_2$ was added to the wells for 30 min at room temperature. The absorbance of the oxidized blue-green product was measured at 405 nm by ELISA reader (BioTek; Winooski, VT, USA).

## Estimation of the Number of Non-Covalently Bound BsAbs per DTX/PIC-Loaded Nanocarriers

On the basis of the literature,[48,49] the surface area of the hydrophilic head-group of phosphatidylcholine (PC) was 0.71 $nm^2$. Then, the diameter of D/P_NCs determined by dynamic light scattering (DLS) was defined as "d". Under the assumption that there were no lipids lost from the D/P_NCs during their preparation, the total number ($N_{tot}$) of phospholipids per D/P_NC was simply calculated using the following formula:

$N_{tot} = 4 \times \pi \times (d/2)^2/0.71$.

The number ($N_{binding}$) of BsAbs per D/P_NCs was calculated using the following formula:

$N_{binding} = N_{tot} \times \varphi/N_{ratio}$;

where $\varphi$ is the molar fraction of DSPE-mPEG2k in D/P_NCs and $N_{ratio}$ is the molar ratio of DSPE-mPEG2k to BsAbs.

## In vitro Stability Studies

To assess the stability of the NCs, the D/P_NCs and Dual-D/P_NCs were diluted in pH 7.4 PBS buffer and stored at 4 °C. The particle size and drug content were monitored with a Zetasizer ZSP (Malvern Instruments, Malvern, UK) and HPLC system to observe colloidal stability of nanocarriers and degradation of the drugs at 0, 24, and 48 h. The critical micelle concentration (CMC) was evaluated using the Zetasizer ZSP (Malvern Instruments, Malvern, UK), which was equipped with a 10 mW He-Ne laser operating at a wavelength of 633 nm, and the detection angle was set at 173° as described in previous reports[50,51] at 25 °C. The D/P_NCs stock solutions were serially diluted to the concentration range of 0.0073~1.875 μg/mL. The CMC was estimated by the intersection of the two straight lines obtained by linear regression of the intensity-concentration plot.

## The Examination of in-vitro Release of Docetaxel and Pictilisib

Drug release profiles of DTX and PIC were studied in 0.5% Tween 80 in pH 7.4 PBS. The free DTX and free PIC solutions were respectively prepared by dissolving the substances in 50/50 (v/v) polysorbate 80/dehydrated alcohol. One milliliter of the DTX and/or PIC solution, DTX and/or PIC-NCs, Tra-D/P_NC, Per-D/P_NC, or Dual-D/P_NC solutions containing 0.3 mg/mL of drugs was transferred onto a dialysis membrane (MWCO 6k~8k, CelluSep® T1; Orange Scientific, Seguin, TX, USA). Then, the dialysis bag was soaked in a tube containing 30 mL of pH 7.4 PBS supplemented with 0.5% Tween 80 at 37 °C with gentle shaking at 100 rpm. One-milliliter aliquot sample solution was withdrawn from each tube and replaced with 1 mL of fresh PBS buffer at predetermined time intervals (1, 2, 4, 6, 8, 12, and 24 h). The amount of each drug released was measured by HPLC.

## In vitro Cellular Uptake Studies

To assess the effect of the decoration of anti-HER2 BsAbs, the cellular uptake of DIO_NCs with BsAbs was evaluated using fluorescence microscopy and flow cytometry. MCF-7/HER2 and MCF-7 cells were respectively seeded into 12-well plates at $1 \times 10^5$ cells/well at 37 °C for 24 h. Cells were treated with DIO_NCs, Tra-DIO_NCs, Per-DIO_NCs, or Dual-DIO_NCs at the same concentration of 5 μg/mL DIO and incubated for several hours. At predetermined time intervals, the cells were washed with PBS to remove the uninternalized nanocarriers. After staining with Hoechst 33,342, cells were observed by fluorescence microscopy (Cytation 3, BioTek Instruments, Winooski, VT, USA), at predetermined time intervals. The amount of uptake was further quantified by Sony SA3800 Spectral flow cytometer (Sony, Tokyo, Japan).

## In vitro Cytotoxicity

The MTT assay was conducted using the MCF-7/HER2 cell line to examine the cytotoxicity of free drugs and different formulations. MCF-7/HER2 cells were seeded in 96-well plates at a density of $1 \times 10^4$ cells/well at 37 °C for 24 h. After

incubation overnight, cells were treated with free PIC, free DTX, free DTX/PIC, DTX_NCs, PIC_NCs, D/P_NCs, Tra-D/P_NCs, Per-D/P_ NCs, or Dual-D/P_NCs over a concentration range of 1~500 ng/mL to optimize the synergistic antitumor ratio of DTX to PIC and evaluate the cytotoxicity of D/P_NCs with and without BsAbs. After 48 h of incubation, cells were refreshed using the medium with 0.5 mg/mL of the MTT reagent and incubated for 3 h. Formazan crystals were dissolved in 200 μL of DMSO. Then, the absorbance was measured at 550 nm with ELISA reader (Cytation 3; BioTek Instruments, Winooski, VT, USA).

## Animals and Tumor Model

All animal experiments were reviewed and approved by the Institutional Animal Care and Use Committee of Taipei Medical University (LAC-2021-0231) in compliance with the Taiwanese *Animal Welfare Act*. To establish the tumor xenograft model, female nude mice (7 weeks old) were subcutaneously inoculated in the right thigh with $1\times10^6$ human breast cancer MCF-7/HER2 cells. Due to the slow growth rate of MCF-7/HER2 cells, 20 μg of estradiol valerate in sesame oil was subcutaneously injected in the neck of the mice to induce the growth and proliferation of breast cancer cells.[52] The tumor volume (V) was calculated using the formula as follows: $V = L \times W^2/2$, where L and W are the length and width, respectively, of the tumor. When the average tumor volumes reached around 100 mm$^3$, MCF-7/HER2 tumor-bearing mice were used for subsequent studies.

## In vivo Pharmacokinetic (PK) Studies

The pharmacokinetics (PK) studies of DTX and PIC were conducted in female Sprague-Dawley rats (7 weeks old). The rats were intravenously administered with a single dosage of 5 mg/kg body weight (BW) of DTX and/or 2.5 mg/kg BW of PIC via the jugular vein. The experimental groups (*n*=3 rats) included free DTX, free PIC, free DTX/PIC, DTX-NCs, PIC-NCs, D/P-NCs, Tra-D/P-NCs, Per-D/P-NCs, and Dual-D/P-NCs. Blood samples were collected from the jugular vein into heparinized centrifuge tubes at predetermined time intervals (0.25, 0.5, 1, 2,4, 6, 8, 10, 24, and 48 h). Blood samples were further centrifuged at 3000 ×*g* for 10 min at 4 °C to obtain plasma samples. Then, plasma samples were stored at −80 °C until a liquid chromatographic (LC)-tandem mass spectroscopic (MS/MS) analysis by TQ-XS (Waters Corp., Manchester UK). The PK parameters were calculated by a non-compartmental analysis using WinNonlin® (Certara, Princeton, NJ, USA).

## In vivo Biodistribution Studies

To evaluate the biodistribution of DTX and PIC, MCF-7/HER2 tumor-bearing mice were randomly divided into nine groups. Free DTX, free PIC, free DTX/PIC, DTX_NCs, PIC_NCs, D/P_NCs, Tra-D/P_NCs, Per-D/P_NCs, and Dual-D/P_NCs were intravenously injected into mice through the tail vein at the same dosage as further studies. At predetermined time intervals, the mice were sacrificed and transcardially perfused with cold PBS supplemented with 10 IU/mL heparin. Organs and tumors were harvested and homogenized in PBS. The homogenate was extracted and analyzed by TQ-XS (Waters Corp., Manchester UK).

## In vivo Tumor Inhibition Studies

After the average tumor volumes had reached around 100 mm$^3$, MCF-7/HER2 tumor-bearing mice were randomly assigned to 10 groups (*n*=4): saline, free DTX, free PIC, free DTX/PIC, DTX_NCs, PIC_NCs, D/P_NCs, Tra-D/P_NCs, Per-D/P_NCs, and Dual-D/P_NCs. Mice were intravenously treated four times with formulations equivalent to a dosage of 5 mg/kg BW of DTX and/or 2.5 mg/kg of PIC via the tail vein every 3 days. The tumor volume and BW of mice were monitored every 3 days. After treatment for 24 days, all mice were sacrificed; the tumor tissues and major organs were harvested and weighed for subsequent studies.

## Biosafety Examination

On day 28 after administration, tumors and organs harvested from previous tumor-inhibition studies were immediately fixed in a 4% paraformaldehyde solution. Fixed tumors and organs were paraffin-embedded, sectioned, and stained with hematoxylin and eosin (H&E). H&E-stained slides were examined using a TissueFAXS microscope (TissueGnostics GmbH, Vienna, Austria).

## Statistical Analysis

All values were presented as the mean±standard deviation (SD). Statistical differences were determined by a one-way analysis of variance (ANOVA) followed by Tukey's test. $p$ values of <0.05 were considered to indicate a significant difference.

## Results

## Physical Characterization of DTX/PIC-Loaded Nanocarriers and Dual BsAb-Decorated DTX/PIC-Loaded Nanocarriers

In previous reports,[46,53] we developed a potential lecithin-stabilized micellar drug delivery system (LsbMDDs) to encapsulate DTX. However, the LsbMDDs did not encapsulate PIC very well. This may result from the lower log $P$ of PIC (1.96),[54] compared with that of DTX (4.26).[55] Hence, we modified the formulation by increasing the drug/DSPE-mPEG2K ratio from 1:5 to 1:10. DTX/PIC-loaded nanocarriers (D/P_NCs) were prepared with a single emulsion method. The average particle size, encapsulation efficiency (EE), drug loading (DL) and zeta potential (ZP) of the formulations are shown in Table 1. The nanocarriers successfully encapsulated not only DTX and PIC individually but simultaneously DTX and PIC with high EE and DL values. Formulations with different drug contents showed similar particle sizes and ZPs. The EE and DL of each formulation were around 97% and 5.5%, respectively. The results indicated that the drug content did not significantly affect the physical properties of nanoparticles. Furthermore, after non-covalent modification with BsAbs in PBS, the particle sizes and ZPs of Tra-D/P_NCs, Per-D/P_NCs and Dual-D/P_NCs are presented in Table 2. The ZPs of D/P_NCs became more negative (−39.7±1.1 mV) due to PBS being pH 7.4, whereas the particle size of D/P_NCs in PBS remained the same as that in deionized water, revealing that the buffer and pH did not affect the nanocarriers. A slight increase in particle size and a decrease in the ZP of BsAbs decorated D/P_NCs were observed, which was attributed to the non-covalently bound BsAbs on the surface of the D/P_NCs. Although the binding of BsAbs decreased the zeta potential, it was still more than −30 mV, which is normally considered stable for nanosuspension.[56] As shown in Figure 1A and B, D/P_NCs showed a spherical morphology and uniform size distribution. In contrast, as shown in Figure 1C and D, Dual-D/P_NCs exhibited a slightly rough spherical morphology, which resulted from the BsAb decorations. Changes in the physical characteristics indirectly demonstrated that the BsAbs had successfully bound to the D/P_NCs and altered their physical properties.

**Table 1** Physical Characterization of Docetaxel (DTX)/Pictilisib (PIC)-Loaded Nanocarriers (D/P_NCs)

| Formulation | Particle size (nm) | PI | ZP (mV) | EE (%) | DL (%) |
|---|---|---|---|---|---|
| DTX_NCs | 149.5±1.4 | 0.352±0.022 | −27.2±0.8 | 100.4±9.4 | 5.68±0.51 |
| PIC_NCs | 154.3±3.2 | 0.303±0.035 | −24.3±1.2 | 98.9±0.6 | 5.60±0.03 |
| D/P_NCs | 142.3±1.0 | 0.230±0.008 | −26.5±0.7 | 97.6±7.6 (D) | 5.51±0.30 |
| | | | | 96.8±4.9 (P) | |

**Abbreviations**: PI, polydispersity index; ZP, zeta potential; DL, drug loading; EE, encapsulation efficiency; D: docetaxel; P: pictilisib.

**Table 2** Physical Characterization of Bispecific Antibodies (BsAbs)-Decorated D/P_NCs in Phosphate-Buffered Saline

| Formulation | Particle Size (nm) | P.I. | ZP (mV) |
|---|---|---|---|
| D/P_NCs | 142.0±2.8 | 0.212±0.020 | −39.7±1.1 |
| Tra-D/P_NCs | 147.4±3.7 | 0.270±0.004 | −34.0±1.2 |
| Per-D/P_NCs | 150.3±1.2 | 0.303±0.032 | −34.6±1.3 |
| Dual-D/P_NCs | 148.4±2.8 | 0.268±0.007 | −33.2±0.7 |

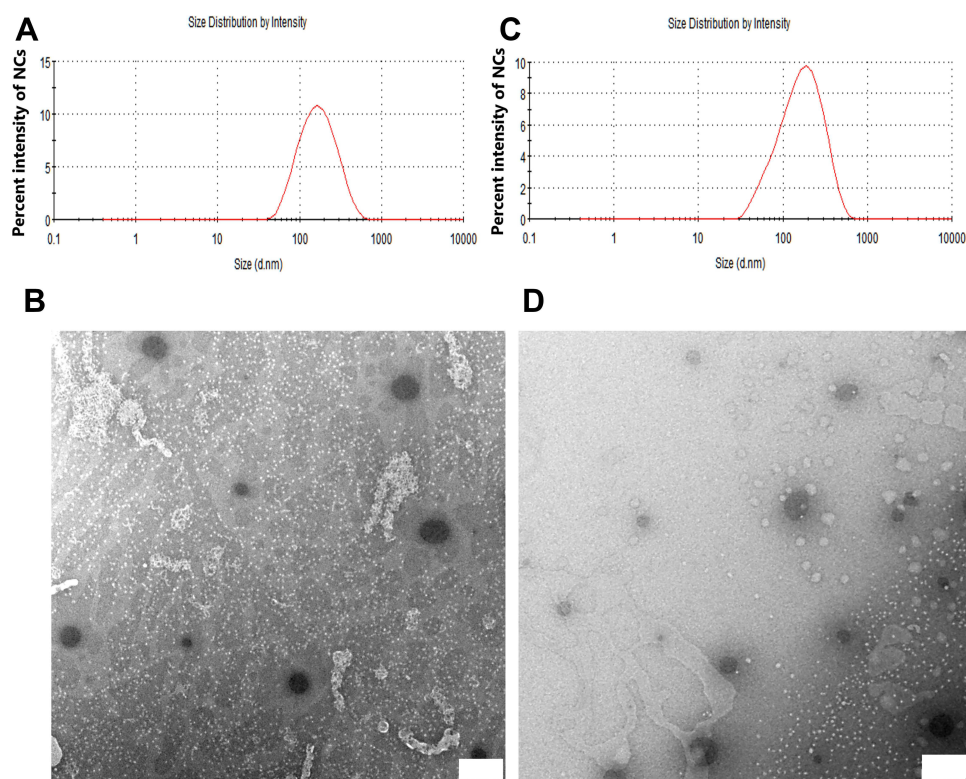**Abbreviations**: PI, polydispersity index; ZP, zeta potential; Tra, trastuzumab; Per, pertuzumab.

**Figure 1** Physical characterization of docetaxel/pictilisib-loaded nanocarriers (D/P_NCs) and Dual-D/P_NCs. The size distribution of (**A**) D/P_NCs and (**C**) Dual-D/P_NCs. TEM images of (**B**) D/P_NCs and (**D**) Dual-D/P_NCs. The scale bar of (**B**) and (**D**) represents 2 μm.

## Evaluation of the Purity and Function of Anti-HER2-IV/mPEG and Anti-HER2-II/mPEG BsAbs

The purity and structural integrity of the BsAbs were examined using SDS-PAGE. As shown in Figure 2A, non-reducing SDS-PAGE showed a single band at ~72 kDa, which was similar to the estimated molecular weight (~74 kDa) and also indicated the integrity and purity of both BsAbs. After reducing the intermolecular and intramolecular disulfide bonds, the reducing SDS-PAGE showed multiple bands at ~55 kDa and ~26 kDa, which represented the high and light chains, respectively, as shown in Figure 2B. MCF-7/HER2 cells and NIH/3T3 cells, as the negative control, were used to evaluate the targeting ability of HER2. The FITC fluorescence intensity of anti-HER2-IV/mPEG (Tra) and anti-HER2-II/mPEG (Per) BsAbs was significantly higher than that of the goat anti-human IgG F(ab')2-FITC alone, as shown in Figure 2C. In a study of NIH/3T3 cells (Figure 2D), the FITC intensity of both BsAbs was similar to that of the goat anti-human IgG F(ab')2-FITC. Besides, the binding specificity of mPEG was investigated with mPEG-coated plates by ELISA. As shown in Figure 2E, the absorbance of Tra and Per BsAbs increased with an increase in the concentration of both BsAbs in mPEG-coated plates; the absorbance of both BsAbs was nearly imperceptible in BSA-coated plates. These results illustrated the structural integrity and binding specificity of both BsAbs, which endowed the D/P_NCs with an active targeting ability to HER2 and mPEG.

## Optimization of the Binding Molar Ratio of BsAbs to DTX/PIC-Loaded Nanocarriers and Estimation of the Number of Non-Covalently Bound BsAbs per DTX/PIC-Loaded Nanocarriers

To confirm whether BsAbs could bind D/P_NCs via the binding ability of mPEG and optimize the binding molar ratio of BsAbs to D/P_NCs, D/P_NCs were incubated with Per BsAbs in various molar ratios of DSPE-mPEG2 to BsAbs of 50:1, 100:1, 500:1, and 1000:1. The excess unbound BsAbs were measured by ELISA method. As illustrated in Figure 3, compared with the BsAbs alone, the absorbance of BsAbs with D/P_NCs was significantly lower, which confirmed that
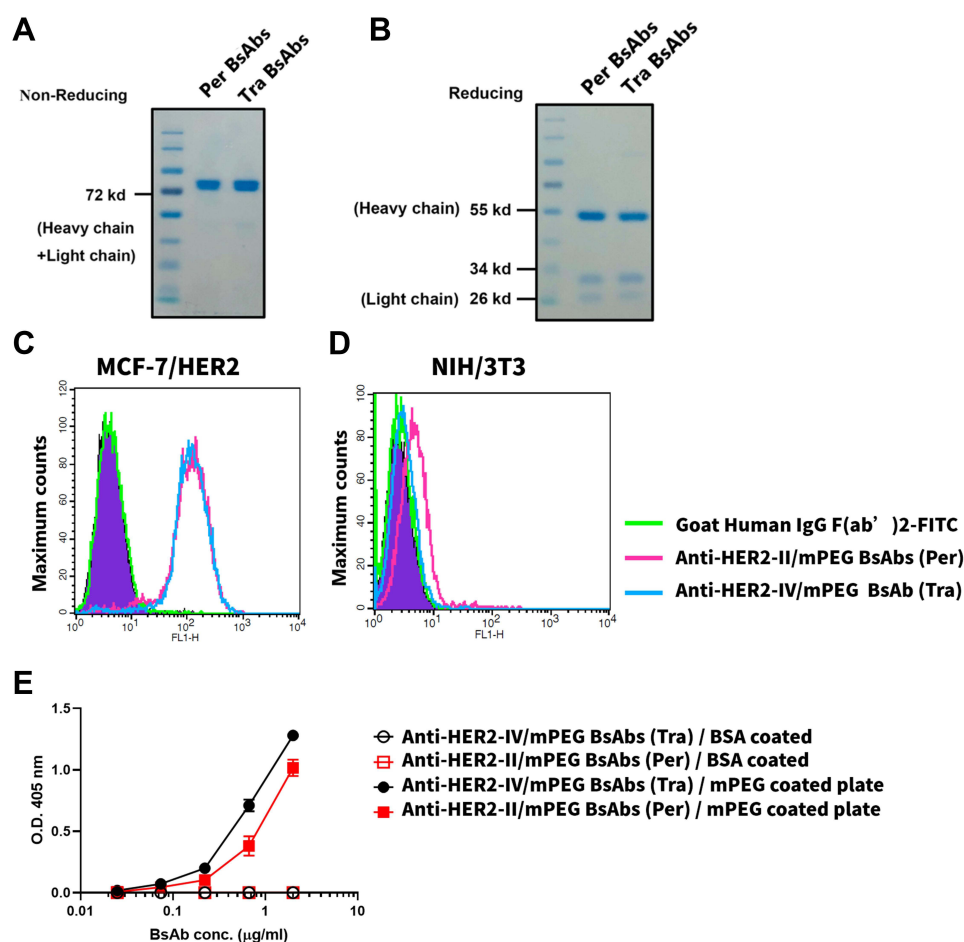
**Figure 2** Characterization of anti-human epidermal growth factor receptor 2 (HER2)-IV/methoxy polyethylene glycol (mPEG) (Tra) and anti-HER2-II/mPEG (Per) bispecific antibodies (BsAbs). The integrity and purity of the BsAbs were evaluated using (**A**) non-reducing SDS-PAGE and (**B**) reducing SDS-PAGE. The binding ability of HER2 was assessed in (**C**) MCF-7/HER2 cells and (**D**) NIH/3T3 cells, and the binding ability of (**E**) mPEG was investigated via ELISA.
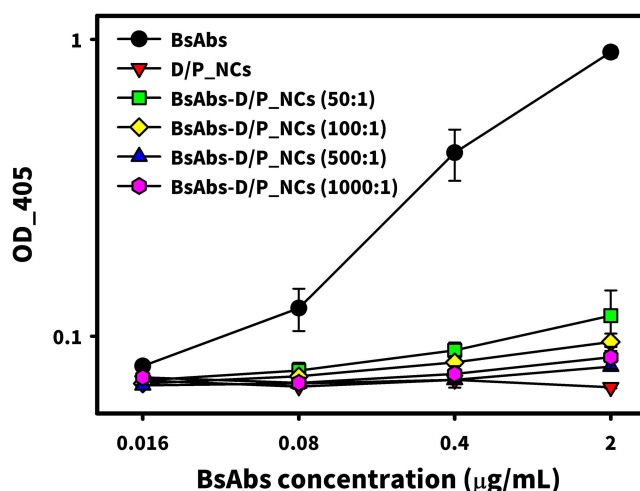


**Figure 3** Evaluation of optimal binding molar ratio of bispecific antibodies (BsAbs) to methoxy polyethylene glycol (mPEG) on docetaxel/pictilisib-loaded nanocarriers (D/P_NCs) by ELISA.

most of the BsAbs had successfully bound to the D/P_NCs via anti-mPEG fragments. Besides, after serial dilution with 2% skimmed milk/PBS, the BsAbs were still tightly decorated on the surface, which indicated that proteins in the skimmed milk did not interfere with the binding of the BsAbs to D/P_NCs. Furthermore, the absorbance of the molar

**Table 3** Estimated Number of Non-Covalently Bound Bispecific Antibodies (BsAbs) per Docetaxel/Pictilisib-Loaded Nanocarriers (D/P_NCs) at Different Molar Ratios

| Group | Numbers of BsAbs per D/P_NCs |
|---|---|
| BsAbs-D/P_NCs (50:1) | 517 |
| BsAbs-D/P_NCs (100:1) | 258 |
| BsAbs-D/P_NCs (500:1) | 52 |
| BsAbs-D/P_NCs (1000:1) | 26 |

ratios of 500:1 and 1000:1 was nearly undetectable, which demonstrated that the maximum binding capacity of BsAbs was approximately 500:1. Based on the particle size of D/P_NCs, we estimated that the total number ($N_{tot}$) of phospholipids per D/P_NCs was approximately 89,599. Under the assumption that there was no lipid loss during the preparation, the number ($N_{binding}$) of BsAbs per D/P_NCs is calculated in Table 3. Results indicated that up to 52 BsAbs could simultaneously bind to a single NP. In contrast to the antibody-drug conjugates (ADCs), the BsAbs-D/P_NCs could load a larger number of different drugs and be armed with versatile targeting ligands. The optimized ratio of 500:1 was used for subsequent experiments to target tumors and reduce costs.

## In vitro Cytotoxicity

The cytotoxic effects of DTX and PIC on MCF-7/HER2 cells were investigated using an MTT assay to evaluate the synergistic cytotoxicity. Results are shown in Figure 4, which illustrates the cell viability of MCF-7 cells treated with free drugs, nanoparticles and nanoparticles decorated with BsAbs. As shown in Figure 4A, the combination of DTX and PIC in each ratio exhibited synergistic cytotoxicity against tumor cells. Values of the 50% inhibitory concentration ($IC_{50}$) of DTX and PIC were, respectively,12.50 and 86.75 ng/mL, and $IC_{50}$ values of DTX:PIC (1:2, 1:1, and 2:1) were 14.15, 9.45, and 8.54 ng/mL, respectively. Furthermore, results shown in Figure 4B exhibit similar cytotoxicity levels of the NCs in a dose-dependent manner. According to the combination index (CI) of previous reports,[57] CI values of each combination of free drugs or nanocarriers were calculated, and all CI values were <1, which indicated the synergistic anticancer effect of the drug combination, as illustrated in Table 4. Due to the lowest $IC_{50}$ and synergistic cytotoxicity of DTX:PIC (2:1), the combination of DTX:PIC at 2:1 ratio was chosen for subsequent studies, which was also consistent with previous reports.[58,59] Moreover, as shown in Figure 4C, decoration of BsAbs onto the D/P_NCs slightly increased the cytotoxicity of DTX/PIC-NPs. The $IC_{50}$ values of BsAbs-D/P_NCs were ~8 ng/mL, which was lower than that of D/P_NCs (9.84 ng/mL). The increase in cytotoxicity may have resulted from the higher cellular uptake of BsAbs-D/P_NCs. Results demonstrated the synergistic tumor inhibition of the combination of DTX and PIC. Results also illustrated that anti-HER2 BsAbs could increase the cytotoxicity of D/P_NCs.
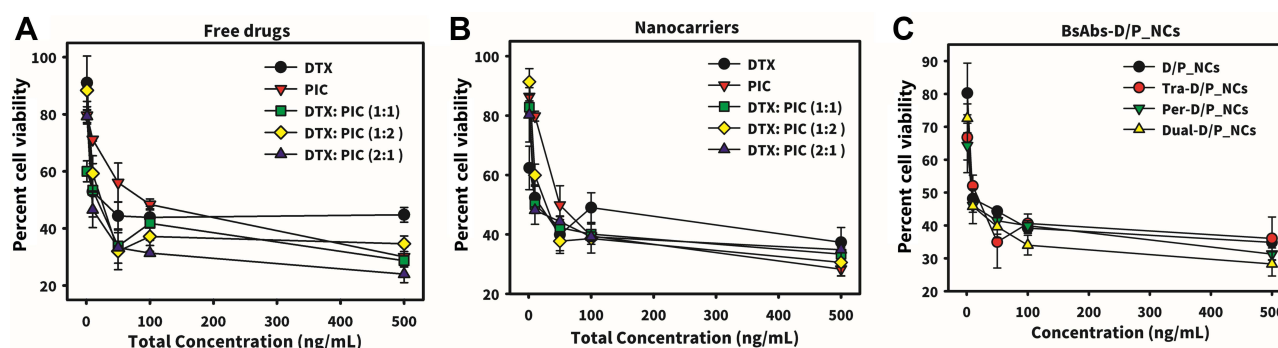


**Figure 4** In vitro cytotoxicity of (**A**) free drugs, (**B**) nanocarriers, and (**C**) bispecific antibodies (BsAbs)-docetaxel/pictilisib-loaded nanocarriers (D/P_NCs) against MCF-7/HER2 cells with incubation for 72 h.

**Table 4** 50% Inhibitory Concentration (IC$_{50}$) and Combination Index (CI) of the Free Drug and Formulations of Docetaxel (DTX) and Pictilisib (PIC)

| | IC$_{50}$ (ng/mL) | | CI | |
|---|---|---|---|---|
| | **Free Drug** | **Nanocarriers** | **Free Drug** | **Nanocarriers** |
| DTX | 12.50±2.69 | 11.29±7.89 | – | – |
| PIC | 86.75±17.56 | 48.91±10.96 | – | – |
| DTX:PIC = 1:1 | 9.45±5.06 | 11.15±7.90 | 0.43 | 0.61 |
| DTX:PIC = 1:2 | 14.15±3.93 | 16.20±3.02 | 0.52 | 0.70 |
| DTX:PIC = 2:1 | 8.54±2.92 | 9.84±1.14 | 0.49 | 0.65 |
| Tra-D/P_NCs | - | 7.63±0.71 | - | - |
| Per-D/P_NCs | - | 7.05±2.13 | - | - |
| Dual-D/P_NCs | - | 8.22±2.21 | - | - |

**Abbreviations**: D, DTX; P, PIC; Tra, trastuzumab; Per, pertuzumab.

## In vitro Stability Studies

The in vitro stability studies of BsAbs-D/P_NCs were conducted in pH 7.4 PBS and monitored for 48 h. As depicted in Figure 5A, there was no obvious changes in either the particle sizes or precipitation of D/P_NCs, Tra-D/P_NCs, Per-D/P_NCs, and Dual-D/P_NCs observed during the experiments, which were all around 150 nm. In addition, both drug assays of each formulation were maintained during storage in physiologic pH buffer as shown in Figure 5B and C. Although the non-covalent decoration of BsAbs slightly altered the physical properties of D/P_NCs, it did not influence the stability of D/P_NCs. Furthermore, CMC studies were conducted to evaluate the colloidal stability of D/P_NCs upon severe dilution in the blood circulation. As depicted in Figure 5D, the intensity of scattered light showed a linear increase with an increase in the concentration, when the concentration was above the CMC. The CMC of D/P_NCs obtained from the intensity-concentration plot was approximately 0.02 μg/mL for the drug concentration and 0.03 μM for the DSPE-mPEG2k concentration, which was almost two orders of magnitude lower than that of DSPE-mPEG2k (2.44 μM) and also significantly lower than other lipids and copolymeric micelles.[60–62] This result demonstrated that the combination of lecithin and DSPE-mPEG2k significantly improved the colloidal stability, which indicated that the NCs would exhibit exceptional stability upon extreme dilution in the blood circulation.

## The Examination of in-vitro Release of Docetaxel and Pictilisib

Drug release profiles of DTX and PIC were examined at pH 7.4 in PBS with 0.5% Tween 80. The cumulative release of DTX in each group reached a plateau within 24 h at around 70% as shown in Figure 6A, whereas the release profile of free DTX/PIC was slower than that of free DTX. In contrast, the cumulative release of PIC reached a plateau within 12 h, and the release profile of the free-drug combination was higher than that of the free PIC, which was distinct from free DTX as shown in Figure 6B. Respective pKa values of DTX and PIC were 10.97[63] and 13.19,[64] and these results indicated that acid-base reactions between DTX and PIC affected the release rate. Additionally, precipitation in the free PIC group was observed in the dialysis bag after 12 h, while precipitation did not occur in the NP groups, which indicated the stability of the NPs, and was consistent with the in vitro stability results. In addition, solubilization of the NPs exhibited significantly increased release rates compared with that of the free drugs, and the non-covalent binding of BsAbs did not alter the drug release rate of DTX or PIC.

## In vitro Cellular Uptake Studies

To evaluate the effect of the decoration of BsAbs on cellular uptake, MCF-7/HER2 cells were incubated with DIO_NCs with or without BsAb decoration for several hours. At predetermined time intervals, cells were analyzed by fluorescence microscopy and flow cytometry. As shown in Figure 7A and B, the fluorescence images revealed that the cellular uptake of DIO_NCs increased with an increasing incubation time and with the non-covalent conjugation of BsAbs. As illustrated in Figure 7C, after incubation for 3 h, all three DIO_NCs with decoration of BsAbs exhibited higher fluorescence intensity, and especially those of
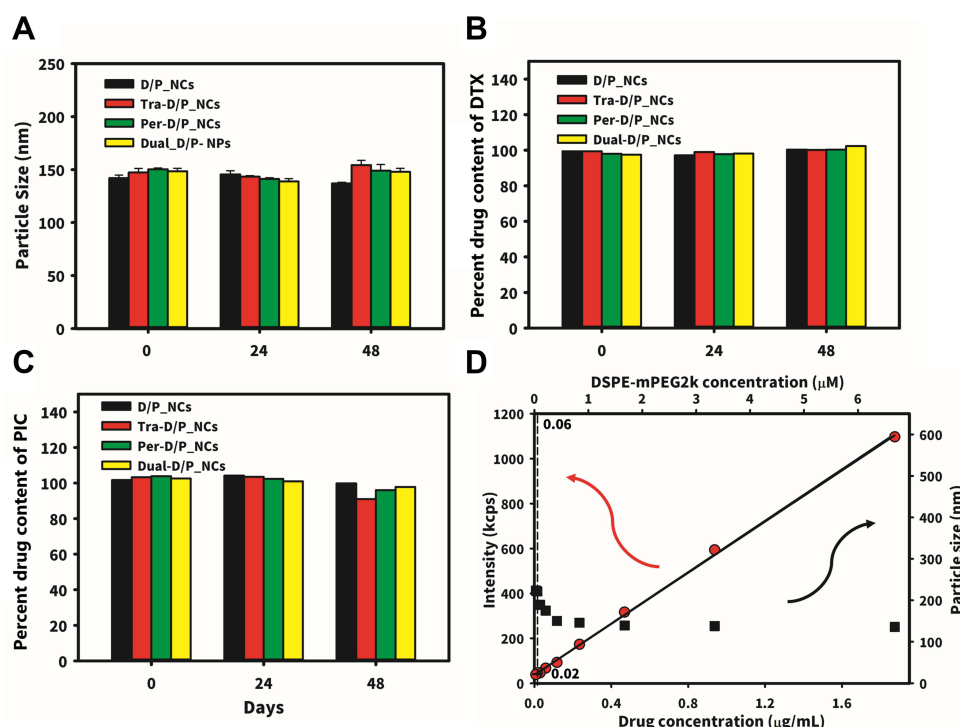
**Figure 5** In vitro stability experiments of D/P_NCs decorated with bispecific antibodies (BsAbs) at 4 °C. (**A**) The particle size, (**B**) DTX assay, and (**C**) PIC assay of D/P_NCs were monitored for 48 h. (**D**) The critical micelle concentration (CMC) was determined to evaluate the colloidal stability after several dilutions using dynamic light scattering (DLS). (estimated CMC = 0.02 μg/mL).
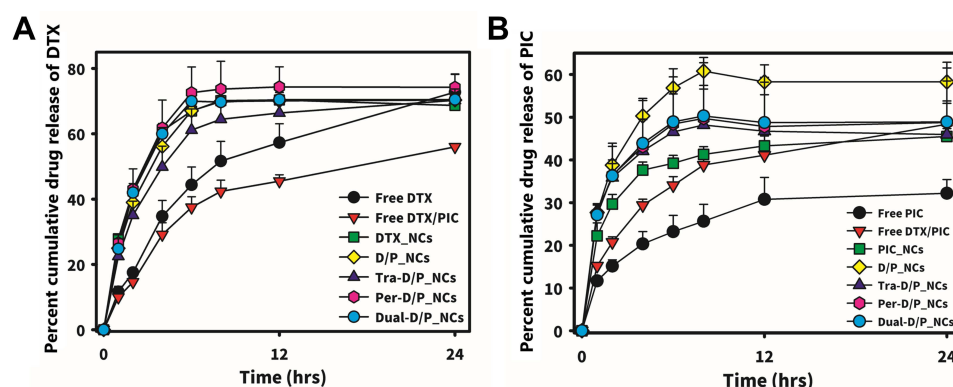


**Figure 6** In vitro drug release profiles of (**A**) docetaxel (DTX) and (**B**) pictilisib (PIC) of free drugs, nanocarriers (NCs), and BsAbs-D/P_NCs.

Per-DIO_NCs and Dual-DIO_NCs were significantly ($p<0.05$) higher than that of DIO_NCs. Correspondingly, after incubation for 24 h, compared with DIO_NCs alone, the fluorescence intensity of all DIO_NCs groups with BsAbs was significantly ($p<0.05$) higher, and the combination of Tra and Per BsAbs exhibited synergistic enhancement of the cellular uptake by targeting complementary subdomains of HER2, which increased the fluorescence intensity by two-fold. Furthermore, MCF-7 cells, wild-type HER2-expressing cells, were also used to assess cellular uptake. In contrast with results in MCF-7/HER2 cells, Tra-DIO_NCs and Per-DIO_NCs did not exhibit a significant increase in the fluorescence intensity compared with DIO_NCs, as depicted in Figure 7D. Nevertheless, Dual-DIO_NCs still showed a significantly ($p<0.05$) higher intensity at both time points, which demonstrated that Tra BsAbs plus Per BsAbs still synergistically increased cellular uptake of the NCs. This result indicated that the chemodrug-loaded nanocarriers decorated with dual HER2 instinct epitopes BsAbs could be also applied to treat HER2-low breast cancer. Results demonstrated that antibody non-covalent functionalization enhanced the cellular uptake of nanoparticles, which might have contributed to the increase in tumor accumulation.
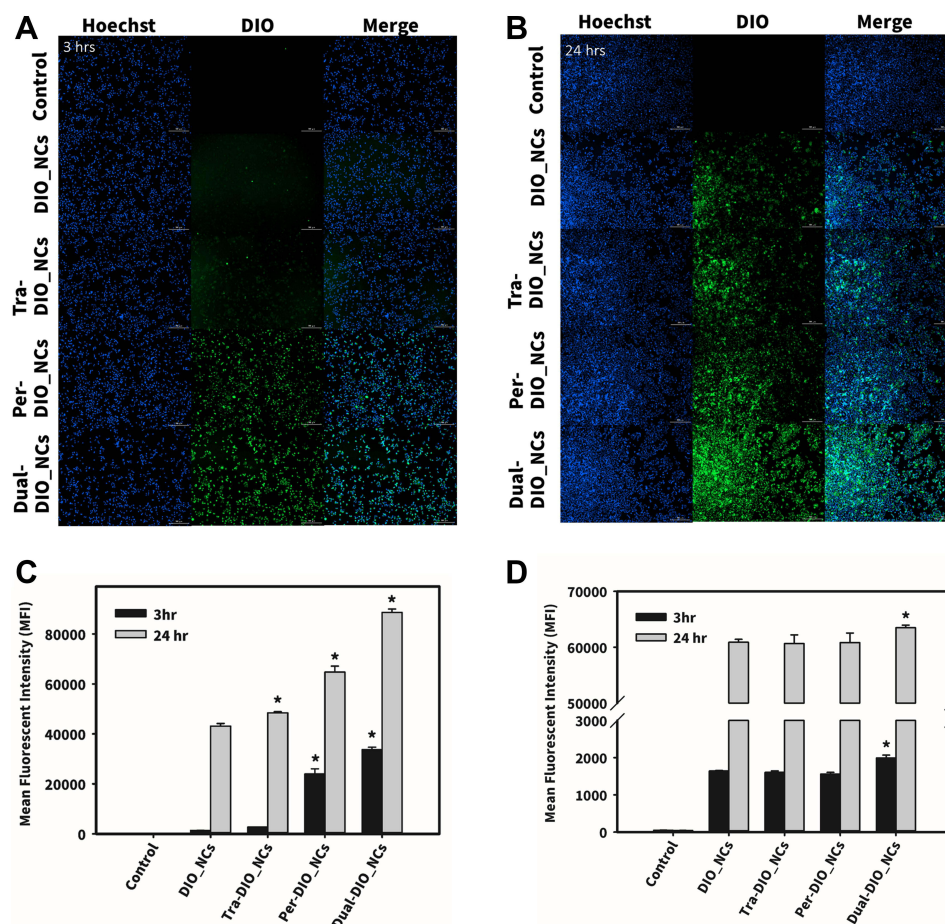
**Figure 7** In vitro cellular uptake studies of MCF-7/human epidermal growth factor receptor 2 (HER2) and MCF-7 cells. Fluorescence images of MCF-7/HER2 cells respectively treated with DIO-loaded nanocarriers (DIO_NCs), trastuzumab (Tra)-DIO_NCs, pertuzumab (Per)-DIO_NCs, and Dual-DIO_NCs were recorded after (**A**) 3 and (**B**) 24 h of incubation. The mean fluorescence intensity of (**C**) MCF-7/HER2 and (**D**) MCF-7 cells treated with formulations was quantified at predetermined time points. * $p<0.05$ compared with DIO_NCs (scale bar 300 μm).

## In vivo Pharmacokinetics Studies

Female SD rats were intravenously administered in each treatment group, and blood samples were collected at predetermined time points. As shown in Figure 8A and Table 5, DTX of free DTX and free DTX/PIC was rapidly cleared from the blood circulation. In contrast, NCs with or without BsAb decoration exhibited significantly prolonged circulation with larger values of
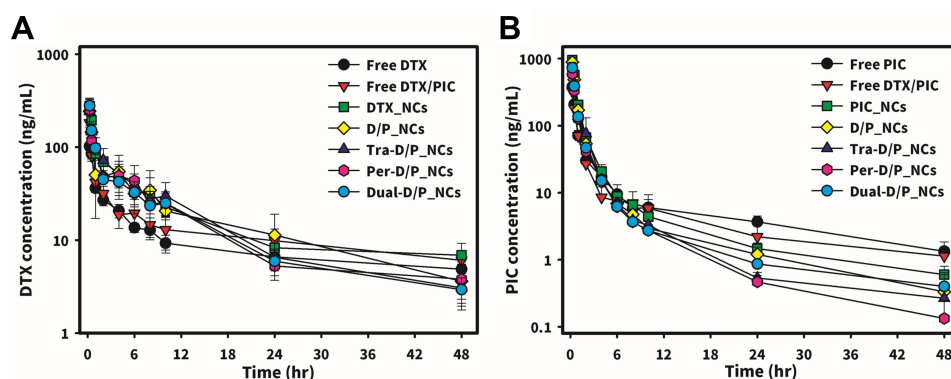


**Figure 8** The plasma concentrations of (**A**) docetaxel (DTX) and (**B**) pictilisib (PIC) over time after the intravenous injection of free drugs, nanocarriers (NCs), and BsAbs-D/P_NCs at the respective DTX and PIC doses of 5 and 2.5 mg/kg.

**Table 5** Pharmacokinetic Parameters of Docetaxel (DTX) Following IV Administrations of Different Formulations at a Dose of 5 mg/kg Body Weight in Rats (n = 3)

| Parameter | Free DTX | Free DTX/PIC | DTX_NCs | D/P_NCs | Tra-D/P_NCs | Per-D/P_NCs | Dual-D/P_NCs |
|---|---|---|---|---|---|---|---|
| $C_0$ (μg/mL) | 0.123±0.04 | 0.436±0.227 | 0.399±0.130 | 0.450±0.245 | 0.414±0.100 | 0.572±0.373 | 0.518±0.140 |
| $t_{1/2}$ (h) | 5.32±0.24 | 6.11±2.36 | 7.65±1.54 | 7.88±1.41 | 5.85±1.20 | 6.41±0.77 | 7.52±1.19 |
| $AUC_{0-last}$ (h×μg/mL) | 0.487±0.037 | 0.659±0.050 | 0.986±0.177 | 0.897±0.215 | 0.928±0.145 | 0.849±0.031 | 0.826±0.087 |
| $AUC_{0-inf}$ (h×μg/mL) | 0.524±0.037 | 0.713±0.071 | 1.064±0.219 | 0.941±0.243 | 0.954±0.144 | 0.883±0.042 | 0.859±0.100 |
| CL (L/h/kg) | 9.58±0.70 | 7.06±0.66 | 4.82±0.89 | 5.59±1.61 | 5.33±0.87 | 5.67±0.27 | 5.88±0.72 |
| Vd (L/kg) | 73.43±5.22 | 60.77±17.43 | 52.09±6.54 | 61.62±7.78 | 44.40±7.13 | 52.67±8.62 | 63.13±6.46 |
| Relative bioavailability (%) | 100 | 136 | 203 | 180 | 182 | 169 | 164 |

**Note**: Values are the mean±standard deviation.
**Abbreviations**: $C_0$, initial plasma concentration; $C_{max}$, highest observed plasma concentration; $t_{1/2}$, elimination half-life; $AUC_{0-last}$, area under the plasma concentration–time curve from 0 h to the last sampling time point; $AUC_{0-inf}$, area under plasma concentration–time curve extrapolated to infinity; CL, plasma clearance; Vd, apparent volume of distribution; PIC, pictilisib; NCs nanocarriers; D, DTX; P, PIC; Tra, trastuzumab; Per, pertuzumab.

the area under the curve (AUC), which increased the relative bioavailability by more than 50%. Furthermore, the initial concentration ($C_0$) of ~1 μg /mL of the NCs groups increased which was significantly higher than ~0.5 μg/mL of free PIC and free DTX/PIC, as shown in Figure 8B and Table 6. Similarly, the AUC values and relative bioavailability of the NCs groups increased compared with the free drug groups. In addition, results of free DTX/PIC indicated drug–drug interactions between DTX and PIC, which corresponded to results of the drug release studies. Importantly, results demonstrated that the NCs improved the circulation of both drugs and the BsAb decoration did not significantly affect the PK profile, which was consistent with the stability studies.

## In vivo Biodistribution Studies

We further investigated whether the NCs and the decoration of BsAbs could improve the tumor accumulation of DTX and PIC in mice. As illustrated in Figure 9A, there was no significant difference observed among the major organs. In contrast, the tumor accumulation of the NCs appeared to have increased. In particular, the accumulation of Tra-D/P_NCs and Dual-D/P_NCs appeared to have been significantly ($p<0.05$) enhanced compared with free DTX. At 8 h after administration, all treatments showed similar accumulation levels of DTX in major organs except for the free DTX group, as shown in Figure 9B. The free DTX group showed higher accumulation in the liver and kidneys, which might be attributed to systemic toxicity. Furthermore, as for PIC, the nanocarriers groups showed transiently higher accumulations in most organs except for the lungs, compared with the free drug groups, as depicted in Figure 9C. Nonetheless, the NCs also enhanced the accumulation of PIC in

**Table 6** Pharmacokinetic Parameters of Pictilisib (PIC) Following IV Administrations of Different Formulations at a Dose of 2.5 mg/kg Body Weight in Rats (n = 3)

| Parameter | Free PIC | Free DTX/PIC | PIC_NCs | D/P_NCs | Tra-D/P_NCs | Per-D/P_NCs | Dual-D/P_NCs |
|---|---|---|---|---|---|---|---|
| $C_0$ (μg/mL) | 0.691±0.115 | 0.587±0.049 | 1.616±0.355 | 1.633±0.351 | 0.997±0.131 | 1.059±0.085 | 1.483±0.844 |
| $t_{1/2}$ (h) | 2.92±0.97 | 2.63±0.41 | 2.84±0.26 | 2.68±0.16 | 2.74±0.25 | 2.40±0.02 | 2.53±0.58 |
| $AUC_{0-last}$ (h×μg/mL) | 0.530±0.046 | 0.438±0.048 | 0.992±0.040 | 0.864±0.123 | 0.701±0.033 | 0.609±0.099 | 0.730±0.099 |
| $AUC_{0-inf}$ (h×μg/mL) | 0.536±0.044 | 0.442±0.048 | 0.994±0.040 | 0.866±0.123 | 0.702±0.033 | 0.610±0.100 | 0.731±0.100 |
| CL (L/h/kg) | 4.69±0.40 | 5.70±0.63 | 2.52±0.10 | 2.93±0.45 | 3.57±0.17 | 4.18±0.72 | 3.46±0.46 |
| Vd (L/kg) | 19.69±6.27 | 21.53±3.10 | 10.32±1.28 | 11.30±1.69 | 14.03±0.65 | 14.48±2.61 | 12.41±1.51 |
| Relative bioavailability (%) | 100 | 83 | 185 | 162 | 131 | 114 | 136 |

**Note**: Values are the mean±standard deviation.
**Abbreviations**: $C_0$, initial plasma concentration; $C_{max}$, highest observed plasma concentration; $t_{1/2}$, elimination half-life; $AUC_{0-last}$, area under plasma concentration–time curve from 0 h to the last sampling time point; $AUC_{0-inf}$, area under plasma concentration–time curve extrapolated to infinity; CL, plasma clearance; Vd, apparent volume of distribution; DTX, docetaxel; NCs, nanocarriers; D, FTX, P, PIC; Tra, trastuzumab; Per, pertuzumab.
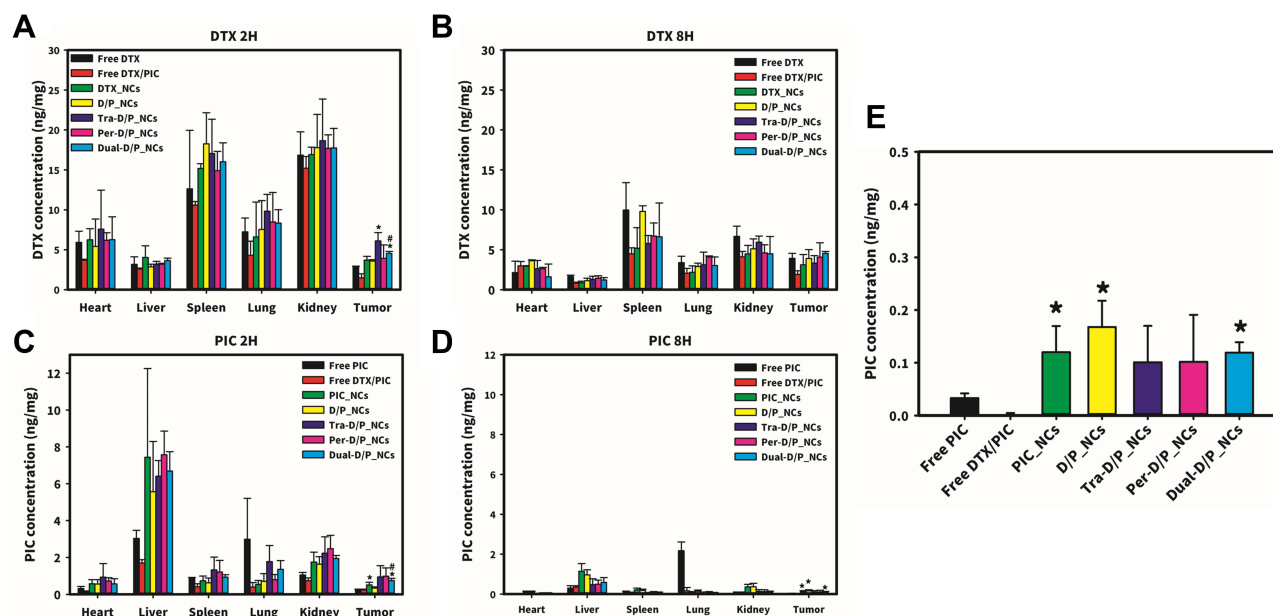
**Figure 9** Biodistribution profiles of major organs and tumors. Docetaxel (DTX) concentrations at (**A**) 2 and (**B**) 8 h after intravenous injection of each formulation in MCF-7/human epidermal growth factor receptor 2 (HER2) tumor-bearing mice. Pictilisib (PIC) concentrations at (**C**) 2 and (**D**) 8 h after intravenous administration in MCF-7/HER2 tumor-bearing mice. (**E**) The PIC concentration of tumors of each treatment group at 8 h after intravenous administration. * $p < 0.05$ compared with PBS group; # $p < 0.05$ compared to the DTX/PIC-loaded (D/P)_nanocarriers (NCs) group.

tumors, and all BsAbs-D/P_NCs groups revealed higher accumulations than the NCs alone in tumors. After 8 h, due to the short half-life of PIC, the concentration of PIC had dramatically declined in both organs and tumors as shown in Figure 9D. Similarly, the nanocarriers groups exhibited significantly ($p<0.05$) higher accumulation in tumors compared with free drug groups, as illustrated in Figure 9E. Besides, PIC concentrations in the reticuloendothelial organs, including the liver, spleen, and kidneys, of the BsAbs-D/P_NCs groups were lower than those of nanocarriers alone. These results revealed that the non-covalent decoration of BsAbs enabled the NCs to escape the immune system. Additionally, the Dual-D/P_NCs showed significantly ($p<0.05$) higher tumor accumulations of both drugs after 2 h compared to the NC groups, which demonstrated that the arming of anti-HER2 BsAbs increased tumor accumulation and was consistent with the results of cellular uptake studies.

## In vivo Tumor Inhibition Studies

MCF-7/HER2 tumor-bearing mice were used to evaluate whether the combination of DTX and PIC and the active targeting ability of the BsAbs resulted in better in vivo therapeutic efficacy. After treatment, the different treatment groups exhibited inhibition of tumor growth, except for the free PIC-treated group, as shown in Figure 10A. Compared with PBS groups, tumor volumes of Tra-D/P_NC-treated, Per-D/P_NC-treated, and Dual-D/P_NC-treated groups had significantly decreased ($p<0.05$), resulting in around 50% inhibition of tumor growth. In addition, there was no significant loss of BW in any groups during the observation, indicating the safety of the treatments, as shown in Figure 10B. Furthermore, on day 24, tumors were harvested for imaging (Figure 10C), and they were weighed to confirm the therapeutic efficacy. As shown in Figure 10D, tumor weights of the free DTX/PIC-treated groups had significantly ($p<0.05$) decreased, which demonstrated the synergistic antitumor effect of the combination of DTX and PIC. In contrast, tumor weights of the free PIC-treated group exhibited little antitumor efficacy, which may be attributed to the lower cytotoxicity of PIC. Moreover, the NC-treated groups efficiently eliminated tumor cells, and BsAb-D/P_NCs-treated groups exhibited significant ($p<0.05$) tumor inhibition, compared with the PBS group. In particular, Dual-D/P_NCs induced 85% inhibition of tumor growth, and the tumor volume of the Dual-D/P_NCs-treated group even showed a significant ($p<0.05$) decrease compared with that of the D/P_NCs-treated group, which resulted from the active targeting ability of both BsAbs and the enhancement of cellular uptake. In conclusion, these results demonstrated the synergistic antitumor effect of the combination of DTX and PIC and an increase in the
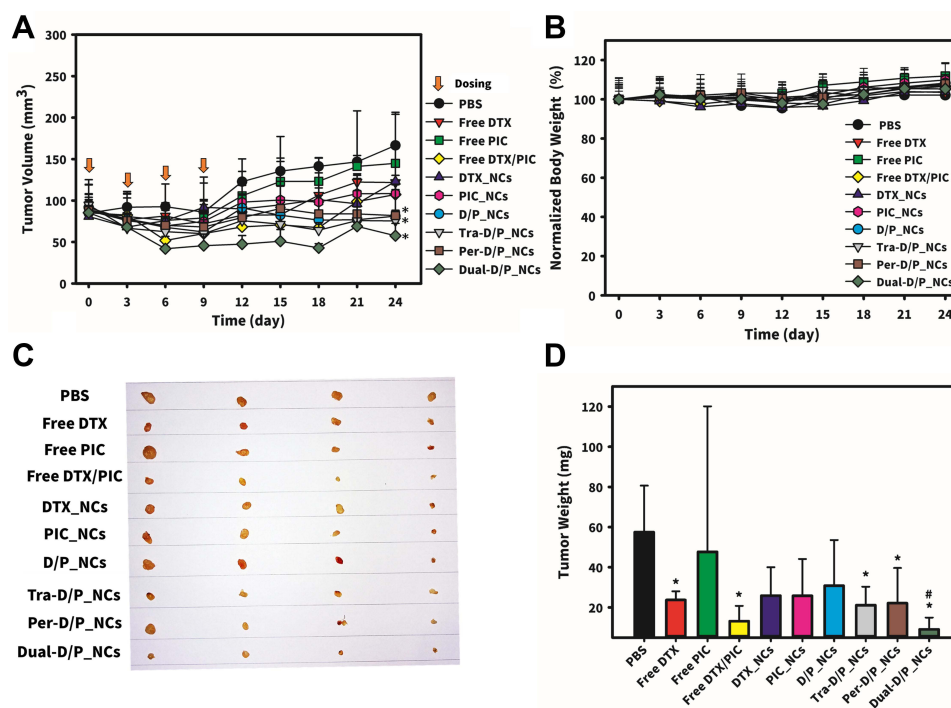
**Figure 10** In vivo evaluation of the antitumor efficacy. (**A**) The average tumor volume in mice bearing MCF-7/human epidermal growth factor receptor 2 (HER2) tumors after intravenous administration in different groups (Q3D×4). (**B**) Body weights of all treatment groups were recorded for 24 days. Tumors were harvested from mice bearing MCF-7/HER2 tumors on day 24. (**C**) Tumor images and (**D**) tumor weights were determined from each treatment group. * $p<0.05$ compared with PBS group; #$p<0.05$ compared with D/P_NCs group.

targeting ability from the non-covalent decoration of BsAbs which efficiently inhibited tumor growth while showing unobvious toxicity.

## Biosafety Examination

On day 24 after the Q3D×4 regimen, tails of free DTX/PIC-treated mice showed severe extravasation injury, commonly induced by chemotherapy,[65] but tails of D/P_NCs group showed no apparent abnormalities, as shown in Figure 11A and B. In addition, there were no obvious abnormalities or lesions observed in H&E-stained heart, spleen, lung, or kidney samples, as shown in Figure 11C, which indicated that DTX and PIC caused little toxicity to these organs. Nonetheless, inflammatory cell infiltration in the liver was observed in H&E-stained free DTX-treated and free DTX/PIC-treated mice, which indicated that free DTX resulted in slight liver damage, and free DTX/PIC led to mild liver injury. In contrast, no obvious inflammatory cell infiltration was observed in the NCs-treated groups, indicating that liver damage deteriorated with the combination of free DTX and PIC, and NCs could alleviate liver damage from the chemodrugs. These results indicated that the encapsulation in NCs and the targeting ability of BsAbs enhanced the therapeutic efficacy while maintaining biosafety.

## Discussion

HER2-positive breast cancer is a highly aggressive cancer and is associated with increased risks of systemic metastasis, recurrence, and mortality.[66] In addition, HER2 overexpression also confers the chemoresistance in breast cancer through several mechanism, including upregulation of drug efflux pumps and drug metabolism proteins and activation of HER2/PI3K/Akt pathway, resulting in multiple drug resistance (MDR).[67,68] Despite the 5-year survival rate of HER2-positive breast cancer has substantially improved with the combination of chemotherapy and HER2-targeted treatments,[69] the increase of the incidence rate and the high mortality rate of breast cancer have led to the urgent need to develop more-effective treatments. Besides, PI3K mutations usually occur in HER2-positive breast cancer, resulting in PI3K/AKT hyperactivation and resistance to chemotherapy and HER-targeted therapy.[70,71] Therefore, several PI3K inhibitors
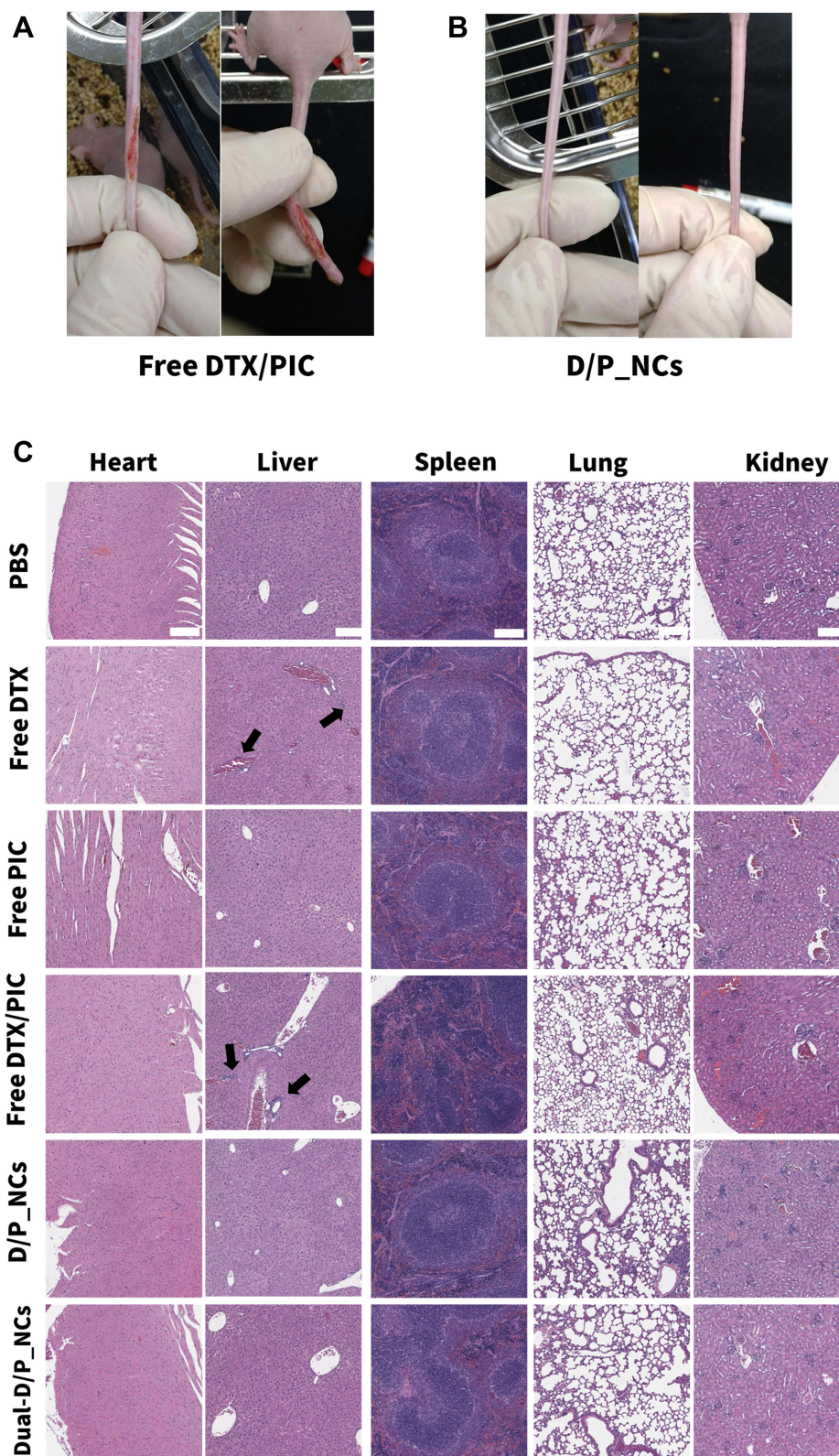
**Figure 11** Biosafety evaluation of nanocarriers (NCs). Tail morphology of (**A**) free docetaxel/pictilisib (DTX/PIC)-treated mice and (**B**) DTX/PIC-encapsulated (D/P)_NCs-treated mice on day 24 after treatment. (**C**) H&E staining of the heart, liver, spleen, lungs, and kidneys. Black arrows indicate inflammatory cell infiltration. (scale bar represents 200 μm).

(PI3Kis) were developed to reverse therapeutic resistance.[72] The PI3K signaling pathway is also involved in regulating the immune system, so PI3Kis were found to act as immunomodulatory agents, which decreased the number of regulatory T (Treg) cells and enhanced CD8^{+} cytotoxic T cells in the tumor microenvironment.[73,74]

In this study, we formulated mPEGylated NCs to simultaneously encapsulate DTX and PIC to achieve a synergistic anticancer effect. Anti-HER2-IV/mPEG and anti-HER2-II/mPEG BsAbs were successfully prepared to non-covalently decorate NCs via the anti-mPEG fragment, which endowed the NCs with a HER2-targeting ability and dual-HER2 blockade via the anti-HER2-IV and anti-HER2-II fragments. Optimal binding studies demonstrated that BsAbs were successfully bound to D/P_NCs, and the binding ability was not interfered with by several dilutions of 2% skimmed milk, which resulted in significant increases of up to two-fold cellular internalization of Dual-D/P_NCs. As previously reported, the decoration of anti-mPEG/anti-tumor antigen bispecific antibody could trigger a rapid cellular internalization of nanocarriers, which contributed to the enhancement of tumor accumulation.[75] Furthermore, the binding synergy of trastuzumab, pertuzumab, and their F(ab')$_2$ fragments was also reported in the previous literature, which showed that binding of trastuzumab enhanced their binding and uptake.[76,77] Moreover, other antibodies were designed to target multiple distinct epitopes of the same receptors, such as insulin-like growth factor-1 receptor (IGF-1R) and death receptor 5 (DR5), which were found to enhance antitumor activity.[78,79] However, the underlying mechanisms still remain to be elucidated, and it is noteworthy to develop more antibodies to distinct epitopes for other receptors and even decorate the nanoparticles to be potent and desired antitumor therapeutics.[79]

The physical characterization and stability of NCs with or without BsAbs showed desired characteristics, including biocompatibility, high encapsulation efficiencies, and suitable particle sizes.[80] The CMC results indicated that the addition of soy lecithin increased the colloidal stability, which was consistent with a previous report.[51] D/P_NCs decorated with BsAbs groups revealed higher cytotoxicity profile than the D/P_NCs alone, which was attributed to the higher cellular uptake of NCs with BsAbs. Nevertheless, the statistical difference of IC$_{50}$ values of each nanocarriers with the combination of DTX and PIC were insignificant, which could be attributed to the reason that the IC$_{50}$ values were below the CMC value.

In vitro cytotoxicity studies revealed that the cytotoxicity of PIC alone was less than that of DTX, whereas the addition of PIC potentiated the cytotoxicity of DTX. The combination of DTX and PIC at a ratio of 2:1 exhibited the synergistic antitumor effect of, which efficiently eliminated the tumor at a lower dose. The latest researches reported that PI3K inhibitors also could augment the cytotoxic response of other chemodrugs, eg, epidermal growth factor receptor (EGFR) kinase inhibitors, topoisomerase II inhibitors, and mitogen-activated protein kinase (MEK) inhibitors, in a variety of cancer, such as triple-negative breast cancer, neuroendocrine cervical cancer, lymphoblastic leukemia.[81–83] PI3K inhibitors have shown several promising therapeutic effects and some of them have been approved by FDA, whereas PI3K inhibitors recently have raised safety concerns about substantial side effects, such as hepatic toxicities, diarrhea, and serious infections.[84] A previous report indicated that PI3K inhibitors can exacerbate liver damage and liver injury via death factor-mediated hepatocyte apoptosis,[85] which was illustrated by obvious deterioration of liver damage of the Free DTX/PIC group in histological stains. However, encapsulation in NCs significantly attenuated hepatotoxicity, which improved the safety and clinical tolerability of PI3K inhibitors, as shown in biosafety studies.

In addition, the nanocarriers decorated with BsAbs showed favorable biodistribution profiles and toxicity profiles. These targeted ligands non-covalently decorate the nanoparticles with specifically designed site-specific domains in thermodynamically favorable interactions, and these were demonstrated to lead to colloidal stabilization and dysopsonization of nanoparticles in a physiological environment.[86,87] In contrast, covalent modification of targeted ligands possibly changed their binding conformations and particle surfaces, resulting in several deleterious effects, including decreases in the binding affinity and colloidal stability.[88,89] Importantly, the NCs efficiently reduced the plasma clearance of DTX and PIC, resulting in a significant increase in the AUC. Our results demonstrated that Dual-D/P_NCs could be a potential anticancer treatment for breast cancer with high biocompatibility, biosafety, and tolerability.

## Conclusions

In summary, we positively established docetaxel/pictilisib-loaded nanocarriers (D/P_NCs) decorated with anti-HER2-IV /mPEG (Tra) and/or anti-HER2-II/mPEG (Per) BsAbs to achieve synergistic targeting and antitumor effects for HER2-positive breast cancer. The in vivo findings also indicated that our nanocarriers could efficiently alleviate the

hepatotoxicity of docetaxel and pictilisib. It highly suggests to apply such a promising platform in clinical applications to overcome the chemical resistance in the treatment of HER2-positive or low-expressed breast cancers.

## Ethical Approval and Consent to Participate

All animal experiments were reviewed and approved by the Institutional Animal Care and Use Committee of Taipei Medical University (LAC-2021-0231) in compliance with the Taiwanese Animal Welfare Act.

## Acknowledgments

## Disclosure

The authors declare no conflicts of interest in this work.

## References

1. Sung H, Ferlay J, Siegel RL., et al. Global Cancer Statistics 2020: GLOBOCAN Estimates of Incidence and Mortality Worldwide for 36 Cancers in 185 Countries. *CA Cancer J Clin*. 2021;71(3):209–249. doi:10.3322/caac.21660
2. Lima SM, Kehm RD, Terry MB. Global breast cancer incidence and mortality trends by region, age-groups, and fertility patterns. *EClinicalMedicine*. 2021;38:100985. doi:10.1016/j.eclinm.2021.100985
3. Iqbal N, Iqbal N. Human Epidermal Growth Factor Receptor 2 (HER2) in Cancers: overexpression and Therapeutic Implications. *Mol Biol Int*. 2014;2014:852748. doi:10.1155/2014/852748
4. Burstein HJ. The distinctive nature of HER2-positive breast cancers. *N Engl J Med*. 2005;353(16):1652–1654. doi:10.1056/NEJMp058197
5. Goutsouliak K, Veeraraghavan J, Sethunath V, et al. Towards personalized treatment for early stage HER2-positive breast cancer. *Nat Rev Clin Oncol*. 2020;17(4):233–250. doi:10.1038/s41571-019-0299-9
6. Loibl S, Gianni L. HER2-positive breast cancer. *Lancet*. 2017;389(10087):2415–2429. doi:10.1016/S0140-6736(16)
7. Oh DY, Bang YJ. HER2-targeted therapies - a role beyond breast cancer. *Nat Rev Clin Oncol*. 2020;17(1):33–48. doi:10.1038/s41571-019-0268-3
8. Wang J, Xu B. Targeted therapeutic options and future perspectives for HER2-positive breast cancer. *Signal Transduct Target Ther*. 2019;4:34. doi:10.1038/s41392-019-0069-2
9. Perez EA, Romond EH, Suman VJ, et al. Trastuzumab plus adjuvant chemotherapy for human epidermal growth factor receptor 2-positive breast cancer: planned joint analysis of overall survival from NSABP B-31 and NCCTG N9831. *J Clin Oncol*. 2014;32(33):3744–3752. doi:10.1200/JCO.2014.55.5730
10. Perez EA, Suman VJ, Davidson NE, et al. Sequential versus concurrent trastuzumab in adjuvant chemotherapy for breast cancer. *J Clin Oncol*. 2011;29(34):4491–4497. doi:10.1200/JCO.2011.36.7045
11. Harbeck N, Gnant M. Breast cancer. *Lancet*. 2017;389(10074):1134–1150. doi:10.1016/S0140-6736(16)
12. Agus DB, Gordon MS, Taylor C, et al. Phase I clinical study of pertuzumab, a novel HER dimerization inhibitor, in patients with advanced cancer. *J Clin Oncol*. 2005;23(11):2534–2543. doi:10.1200/JCO.2005.03.184
13. Nahta R, Hung MC, Esteva FJ. The HER-2-targeting antibodies trastuzumab and pertuzumab synergistically inhibit the survival of breast cancer cells. *Cancer Res*. 2004;64(7):2343–2346. doi:10.1158/0008-5472.can-03-3856
14. Lee-Hoeflich ST, Crocker L, Yao E, et al. A central role for HER3 in HER2-amplified breast cancer: implications for targeted therapy. *Cancer Res*. 2008;68(14):5878–5887. doi:10.1158/0008-5472.CAN-08-0380
15. Scheuer W, Friess T, Burtscher H, Bossenmaier B, Endl J, Hasmann M. Strongly enhanced antitumor activity of trastuzumab and pertuzumab combination treatment on HER2-positive human xenograft tumor models. *Cancer Res*. 2009;69(24):9330–9336. doi:10.1158/0008-5472.CAN-08-4597
16. Swain SM, Baselga J, Kim SB, et al. Pertuzumab, trastuzumab, and docetaxel in HER2-positive metastatic breast cancer. *N Engl J Med*. 2015;372 (8):724–734. doi:10.1056/NEJMoa1413513
17. Goncalves MD, Hopkins BD, Cantley LC. Phosphatidylinositol 3-Kinase, Growth Disorders, and Cancer. *N Engl J Med*. 2018;379(21):2052–2062. doi:10.1056/NEJMra1704560
18. Bahrami A, Khazaei M, Shahidsales S, et al. The Therapeutic Potential of PI3K/Akt/mTOR Inhibitors in Breast Cancer: rational and Progress. *J Cell Biochem*. 2018;119(1):213–222. doi:10.1002/jcb.26136
19. Xu F, Na L, Li Y, Chen L. Roles of the PI3K/AKT/mTOR signalling pathways in neurodegenerative diseases and tumours. *Cell Biosci*. 2020;10 (1):54. doi:10.1186/s13578-020-00416-0
20. Kataoka Y, Mukohara T, Shimada H, Saijo N, Hirai M, Minami H. Association between gain-of-function mutations in PIK3CA and resistance to HER2-targeted agents in HER2-amplified breast cancer cell lines. *Ann Oncol*. 2010;21(2):255–262. doi:10.1093/annonc/mdp304
21. Ellis H, Ma CX. PI3K Inhibitors in Breast Cancer Therapy. *Curr Oncol Rep*. 2019;21(12):110. doi:10.1007/s11912-019-0846-7

22. Vasan N, Toska E, Scaltriti M. Overview of the relevance of PI3K pathway in HR-positive breast cancer. *Ann Oncol*. 2019;30(Suppl_10):x3–x11. doi:10.1093/annonc/mdz281

23. Serra V, Scaltriti M, Prudkin L, et al. PI3K inhibition results in enhanced HER signaling and acquired ERK dependency in HER2-overexpressing breast cancer. *Oncogene*. 2011;30(22):2547–2557. doi:10.1038/onc.2010.626

24. Fujimoto Y, Morita TY, Ohashi A, et al. Combination treatment with a PI3K/Akt/mTOR pathway inhibitor overcomes resistance to anti-HER2 therapy in PIK3CA-mutant HER2-positive breast cancer cells. *Sci Rep*. 2020;10(1):21762. doi:10.1038/s41598-020-78646-y

25. Rexer BN, Chanthaphaychith S, Dahlman K, Arteaga CL. Direct inhibition of PI3K in combination with dual HER2 inhibitors is required for optimal antitumor activity in HER2+ breast cancer cells. *Breast Cancer Res*. 2014;16(1):R9. doi:10.1186/bcr3601

26. Verret B, Cortes J, Bachelot T, Andre F, Arnedos M. Efficacy of PI3K inhibitors in advanced breast cancer. *Ann Oncol*. 2019;30 Suppl 10:x12–x20. doi:10.1093/annonc/mdz381

27. Li H, Prever L, Hirsch E, Gulluni F. Targeting PI3K/AKT/mTOR Signaling Pathway in Breast Cancer. *Cancers*. 2021;13(14):14. doi:10.3390/cancers13143517

28. Sarker D, Ang JE, Baird R, et al. First-in-human phase I study of pictilisib (GDC-0941), a potent pan-class I phosphatidylinositol-3-kinase (PI3K) inhibitor, in patients with advanced solid tumors. *Clin Cancer Res*. 2015;21(1):77–86. doi:10.1158/1078-0432.CCR-14-0947

29. Wallin JJ, Guan J, Prior WW, et al. GDC-0941, a novel class I selective PI3K inhibitor, enhances the efficacy of docetaxel in human breast cancer models by increasing cell death in vitro and in vivo. *Clin Cancer Res*. 2012;18(14):3901–3911. doi:10.1158/1078-0432.CCR-11-2088

30. Yao E, Zhou W, Lee-Hoeflich ST, et al. Suppression of HER2/HER3-mediated growth of breast cancer cells with combinations of GDC-0941 PI3K inhibitor, trastuzumab, and pertuzumab. *Clin Cancer Res*. 2009;15(12):4147–4156. doi:10.1158/1078-0432.CCR-08-2814

31. Wang J, Zhang Y, Xiao Y, et al. Boosting immune surveillance by low-dose PI3K inhibitor facilitates early intervention of breast cancer. *Am J Cancer Res*. 2021;11(5):2005–2024.

32. Narang AS, Chang RK, Hussain MA. Pharmaceutical development and regulatory considerations for nanoparticles and nanoparticulate drug delivery systems. *J Pharm Sci*. 2013;102(11):3867–3882. doi:10.1002/jps.23691

33. Hanafy N. *Development and production of multifunctional bio-nano-engineered drug delivery systems loaded by TGF β1 inhibitors for delivering into hepatocellular carcinoma cells*. Lecce, Italy:Salento University; 2017.

34. Hanafy NAN. Optimally designed theranostic system based folic acids and chitosan as a promising mucoadhesive delivery system for encapsulating curcumin LbL nano-template against invasiveness of breast cancer. *Int J Biol Macromol*. 2021;182:1981–1993. doi:10.1016/j.ijbiomac.2021.05.149

35. Hanafy NAN, Leporatti S, El-Kemary MA. Extraction of chlorophyll and carotenoids loaded into chitosan as potential targeted therapy and bio imaging agents for breast carcinoma. *Int J Biol Macromol*. 2021;182:1150–1160. doi:10.1016/j.ijbiomac.2021.03.189

36. Dang Y, Guan J. Nanoparticle-based drug delivery systems for cancer therapy. *Smart Mater Med*. 2020;1:10–19. doi:10.1016/j.smaim.2020.04.001

37. Anselmo AC, Mitragotri S. Nanoparticles in the clinic: an update post COVID-19 vaccines. *Bioeng Transl Med*. 2021;e10246. doi:10.1002/btm2.10246

38. Bobo D, Robinson KJ, Islam J, Thurecht KJ, Corrie SR. Nanoparticle-Based Medicines: a Review of FDA-Approved Materials and Clinical Trials to Date. *Pharm Res*. 2016;33(10):2373–2387. doi:10.1007/s11095-016-1958-5

39. Sharifyrad M, Gohari S, Fathi M, et al. The efficacy and neuroprotective effects of edaravone-loaded mPEG-b-PLGA polymeric nanoparticles on human neuroblastoma SH-SY5Y cell line as in vitro model of ischemia. *J Drug Deliv Sci Technol*. 2022;73:103378. doi:10.1016/j.jddst.2022.103378

40. Harris JM, Chess RB. Effect of pegylation on pharmaceuticals. *Nat Rev Drug Discov*. 2003;2(3):214–221. doi:10.1038/nrd1033

41. Manjili H, Malvandi H, Mosavi MS, Danafar H. Preparation and Physicochemical Characterization of Biodegradable mPEG-PCL Core-Shell Micelles for Delivery of Artemisinin. *Pharmaceutical Sci*. 2016;22:234–243. doi:10.15171/PS.2016.37

42. Patra JK, Das G, Fraceto LF, et al. Nano based drug delivery systems: recent developments and future prospects. *J Nanobiotechnology*. 2018;16(1):71. doi:10.1186/s12951-018-0392-8

43. Wu D, Si M, Xue HY, Wong HL. Nanomedicine applications in the treatment of breast cancer: current state of the art. *Int J Nanomedicine*. 2017;12:5879–5892. doi:10.2147/ijn.S123437

44. Cohen-Sela E, Teitlboim S, Chorny M, et al. Single and double emulsion manufacturing techniques of an amphiphilic drug in PLGA nanoparticles: formulations of mithramycin and bioactivity. *J Pharm Sci*. 2009;98(4):1452–1462. doi:10.1002/jps.21527

45. Nosrati H, Adinehvand R, Manjili HK, Rostamizadeh K, Danafar H. Synthesis, characterization, and kinetic release study of methotrexate loaded mPEG-PCL polymersomes for inhibition of MCF-7 breast cancer cell line. *Pharm Dev Technol*. 2019;24(1):89–98. doi:10.1080/10837450.2018.1425433

46. Su CY, Chen M, Chen LC, et al. Bispecific antibodies (anti-mPEG/anti-HER2) for active tumor targeting of docetaxel (DTX)-loaded mPEGylated nanocarriers to enhance the chemotherapeutic efficacy of HER2-overexpressing tumors. *Drug Deliv*. 2018;25(1):1066–1079. doi:10.1080/10717544.2018.1466936

47. Kao CH, Wang JY, Chuang KH, et al. One-step mixing with humanized anti-mPEG bispecific antibody enhances tumor accumulation and therapeutic efficacy of mPEGylated nanoparticles. *Biomaterials*. 2014;35(37):9930–9940. doi:10.1016/j.biomaterials.2014.08.032

48. Tansi FL, Ruger R, Bohm C, et al. Activatable bispecific liposomes bearing fibroblast activation protein directed single chain fragment/Trastuzumab deliver encapsulated cargo into the nuclei of tumor cells and the tumor microenvironment simultaneously. *Acta Biomater*. 2017;54:281–293. doi:10.1016/j.actbio.2017.03.033

49. Engelman DM. Surface area per lipid molecule in the intact membrane of the human red cell. *Nature*. 1969;223(5212):1279–1280. doi:10.1038/2231279a0

50. Topel Ö, Çakır BA, Budama L, Hoda N. Determination of critical micelle concentration of polybutadiene-block-poly(ethyleneoxide) diblock copolymer by fluorescence spectroscopy and dynamic light scattering. *J Mol Liq*. 2013;177:40–43. doi:10.1016/j.molliq.2012.10.013

51. Cheng WJ, Chuang KH, Lo YJ, et al. Bispecific T-cell engagers non-covalently decorated drug-loaded PEGylated nanocarriers for cancer immunochemotherapy. *J Control Release*. 2022;344:235–248. doi:10.1016/j.jconrel.2022.03.015

52. Chen M, Sheu MT, Cheng TL, et al. A novel anti-tumor/anti-tumor-associated fibroblast/anti-mPEG tri-specific antibody to maximize the efficacy of mPEGylated nanomedicines against fibroblast-rich solid tumor. *Biomater Sci*. 2021;10(1):202–215. doi:10.1039/d1bm01218e

53. Su CY, Liu JJ, Ho YS, et al. Development and characterization of docetaxel-loaded lecithin-stabilized micellar drug delivery system (LsbMDDs) for improving the therapeutic efficacy and reducing systemic toxicity. *Eur J Pharm Biopharm*. 2018;123:9–19. doi:10.1016/j.ejpb.2017.11.006

54. Han N, Jiang Y, Gai Y, et al. (11)C-Labeled Pictilisib (GDC-0941) as a Molecular Tracer Targeting Phosphatidylinositol 3-Kinase (PI3K) for Breast Cancer Imaging. *Contrast Media Mol Imaging*. 2019;2019:1760184. doi:10.1155/2019/1760184

55. Baek J-S, Cho C-W. Comparison of solid lipid nanoparticles for encapsulating paclitaxel or docetaxel. *J Pharmaceutical Investigation*. 2015;45 (7):625–631. doi:10.1007/s40005-015-0182-3

56. Samimi S, Maghsoudnia N, Eftekhari RB, Dorkoosh F. Chapter 3 - Lipid-Based Nanoparticles for Drug Delivery Systems. In: Mohapatra SS, Ranjan S, Dasgupta N, Mishra RK, Thomas S, editors. *Characterization and Biology of Nanomaterials for Drug Delivery*. Elsevier; 2019:47–76.

57. Chou T-C, Talalay P. Quantitative analysis of dose-effect relationships: the combined effects of multiple drugs or enzyme inhibitors. *Adv Enzyme Regul*. 1984;22:27–55. doi:10.1016/0065-2571(84)90007-4

58. Wang Y, Li J, Chen JJ, Gao X, Huang Z, Shen Q. Multifunctional Nanoparticles Loading with Docetaxel and GDC0941 for Reversing Multidrug Resistance Mediated by PI3K/Akt Signal Pathway. *Mol Pharm*. 2017;14(4):1120–1132. doi:10.1021/acs.molpharmaceut.6b01045

59. Zuo T, Li J, Zhang J, et al. Coadministration of chemotherapy and PI3K/Akt pathway treatment with multistage acidity/CathB enzyme-responsive nanocarriers for inhibiting the metastasis of breast cancer. *Biomater Sci*. 2019;7(12):5054–5067. doi:10.1039/c9bm01348b

60. Mare R, Da H, Fresta M, Cosco D, Awasthi V. Anchoring Property of a Novel Hydrophilic Lipopolymer, HDAS-SHP, Post-Inserted in Preformed Liposomes. *Nanomaterials*. 2019;9(9):548. doi:10.3390/nano9091185

61. Ashok B, Arleth L, Hjelm RP, Rubinstein I, Onyuksel H. In vitro characterization of PEGylated phospholipid micelles for improved drug solubilization: effects of PEG chain length and PC incorporation. *J Pharm Sci*. 2004;93(10):2476–2487. doi:10.1002/jps.20150

62. Hussein YHA, Youssry M. Polymeric Micelles of Biodegradable Diblock Copolymers: enhanced Encapsulation of Hydrophobic Drugs. *Materials*. 2018;11(5):548. doi:10.3390/ma11050688

63. Sohail MF, Rehman M, Sarwar HS, et al. Advancements in the oral delivery of Docetaxel: challenges, current state-of-The-art and future trends. *Int J Nanomedicine*. 2018;13:3145–3161. doi:10.2147/IJN.S164518

64. Wishart DS, Knox C, Guo AC, et al. DrugBank: a comprehensive resource for in silico drug discovery and exploration. *Nucleic Acids Res*. 2006;34 (Databaseissue):D668–72. doi:10.1093/nar/gkj067

65. Kreidieh FY, Moukadem HA, El Saghir NS. Overview, prevention and management of chemotherapy extravasation. *World J Clin Oncol*. 2016;7 (1):87–97. doi:10.5306/wjco.v7.i1.87

66. Gonzalez-Angulo AM, Litton JK, Broglio KR, et al. High risk of recurrence for patients with breast cancer who have human epidermal growth factor receptor 2-positive, node-negative tumors 1 cm or smaller. *J Clin Oncol*. 2009;27(34):5700–5706. doi:10.1200/JCO.2009.23.2025

67. Kang HJ, Yi YW, Hong YB, et al. HER2 confers drug resistance of human breast cancer cells through activation of NRF2 by direct interaction. *Sci Rep*. 2014;4(1):7201. doi:10.1038/srep07201

68. Knuefermann C, Lu Y, Liu B, et al. HER2/PI-3K/Akt activation leads to a multidrug resistance in human breast adenocarcinoma cells. *Oncogene*. 2003;22(21):3205–3212. doi:10.1038/sj.onc.1206394

69. Bradley R, Braybrooke J, Gray R, et al. Trastuzumab for early-stage, HER2-positive breast cancer: a meta-analysis of 13 864 women in seven randomised trials. *Lancet Oncol*. 2021;22(8):1139–1150. doi:10.1016/S1470-2045(21)00288-6

70. O'Brien NA, McDonald K, Tong L, et al. Targeting PI3K/mTOR overcomes resistance to HER2-targeted therapy independent of feedback activation of AKT. *Clin Cancer Res*. 2014;20(13):3507–3520. doi:10.1158/1078-0432.CCR-13-2769

71. Wang Q, Shi YL, Zhou K, et al. PIK3CA mutations confer resistance to first-line chemotherapy in colorectal cancer. *Cell Death Dis*. 2018;9(7):739. doi:10.1038/s41419-018-0776-6

72. Vanhaesebroeck B, Perry MWD, Brown JR, André F, Okkenhaug K. PI3K inhibitors are finally coming of age. *Nat Rev Drug Discov*. 2021;20 (10):741–769. doi:10.1038/s41573-021-00209-1

73. Carnevalli LS, Sinclair C, Taylor MA, et al. PI3Kα/δ inhibition promotes anti-tumor immunity through direct enhancement of effector CD8+ T-cell activity. *J Immuno Therapy Cancer*. 2018;6(1):158. doi:10.1186/s40425-018-0457-0

74. Eschweiler S, Ramírez-Suástegui C, Li Y, et al. Intermittent PI3Kδ inhibition sustains anti-tumour immunity and curbs irAEs. *Nature*. 2022. doi:10.1038/s41586-022-04685-2

75. Su YC, Burnouf PA, Chuang KH, Chen BM, Cheng TL, Roffler SR. Conditional internalization of PEGylated nanomedicines by PEG engagers for triple negative breast cancer therapy. *Nat Commun*. 2017;8:15507. doi:10.1038/ncomms15507

76. Sharma R, Kumbhakar M, Mukherjee A. Toward Understanding the Binding Synergy of Trastuzumab and Pertuzumab to Human Epidermal Growth Factor Receptor 2. *Mol Pharm*. 2021;18(12):4553–4563. doi:10.1021/acs.molpharmaceut.1c00775

77. Fuentes G, Scaltriti M, Baselga J, Verma CS. Synergy between trastuzumab and pertuzumab for human epidermal growth factor receptor 2 (Her2) from colocalization: an in silicobased mechanism. *Breast Cancer Res*. 2011;13(3):R54. doi:10.1186/bcr2888

78. Dong J, Demarest SJ, Sereno A, et al. Combination of two insulin-like growth factor-I receptor inhibitory antibodies targeting distinct epitopes leads to an enhanced antitumor response. *Mol Cancer Ther*. 2010;9(9):2593–2604. doi:10.1158/1535-7163.MCT-09-1018

79. Overdijk MB, Strumane K, Beurskens FJ, et al. Dual Epitope Targeting and Enhanced Hexamerization by DR5 Antibodies as a Novel Approach to Induce Potent Antitumor Activity Through DR5 Agonism. *Mol Cancer Ther*. 2020;19(10):2126–2138. doi:10.1158/1535-7163.Mct-20-0044

80. Tang X, Loc WS, Dong C, et al. The use of nanoparticulates to treat breast cancer. *Nanomedicine*. 2017;12(19):2367–2388. doi:10.2217/nnm-2017-0202

81. Yi YW, Hong W, Kang HJ, et al. Inhibition of the PI3K/AKT pathway potentiates cytotoxicity of EGFR kinase inhibitors in triple-negative breast cancer cells. *J Cell Mol Med*. 2013;17(5):648–656. doi:10.1111/jcmm.12046

82. Lai ZY, Yeo HY, Chen YT, et al. PI3K inhibitor enhances the cytotoxic response to etoposide and cisplatin in a newly established neuroendocrine cervical carcinoma cell line. *Oncotarget*. 2017;8(28):45323–45334. doi:10.18632/oncotarget.17335

83. Cante-Barrett K, Spijkers-Hagelstein JA, Buijs-Gladdines JG, et al. MEK and PI3K-AKT inhibitors synergistically block activated IL7 receptor signaling in T-cell acute lymphoblastic leukemia. *Leukemia*. 2016;30(9):1832–1843. doi:10.1038/leu.2016.83

84. Richardson NC, Kasamon Y, Pazdur R, Gormley N. The saga of PI3K inhibitors in haematological malignancies: survival is the ultimate safety endpoint. *Lancet Oncol*. 2022;23(5):563–566. doi:10.1016/S1470-2045(22)00200-5

85. Liu W, Jing ZT, Xue CR, et al. PI3K/AKT inhibitors aggravate death receptor-mediated hepatocyte apoptosis and liver injury. *Toxicol Appl Pharmacol*. 2019;381:114729. doi:10.1016/j.taap.2019.114729

86. Treuel L, Brandholt S, Maffre P, Wiegele S, Shang L, Nienhaus GU. Impact of Protein Modification on the Protein Corona on Nanoparticles and Nanoparticle–Cell Interactions. *ACS Nano*. 2014;8(1):503–513. doi:10.1021/nn405019v

87. Oh JY, Kim HS, Palanikumar L, et al. Cloaking nanoparticles with protein Corona shield for targeted drug delivery. *Nat Commun*. 2018;9(1):4548. doi:10.1038/s41467-018-06979-4

88. Salvati A, Pitek AS, Monopoli MP, et al. Transferrin-functionalized nanoparticles lose their targeting capabilities when a biomolecule Corona adsorbs on the surface. *Nat Nanotechnol*. 2013;8(2):137–143. doi:10.1038/nnano.2012.237

89. Laga R, Pola R, Ulbrich K, et al. Avidin-conjugated polymers with monobiotinylated antibody fragments: a new strategy for the noncovalent attachment of recombinant proteins for polymer therapeutics. *J Bioact Compat Polym*. 2013;28(3):289–299. doi:10.1177/0883911513486225